Islamic University of Gaza

Faculty of Engineering

Electrical Engineering Department

Design of UMTS/ LTE Diplexer and DCS/ UMTS/ LTE Triplexer For Mobile Communication Systems

By

Anas F. Al-ghoul

Supervisor

Dr. Talal F. Skaik

A Thesis Submitted in Partial Fulfillment of the Requirements for the Degree of Master in Electrical/Communication Engineering Faculty of Engineering

1434هـ – 2013 م

إقـــــرار

أنا الموقع أدناه مقدم الرسالة التي تحمل العنوان:

Design of UMTS/ LTE Diplexer and DCS/ UMTS/ LTE Triplexer For Mobile Communication Systems

أقر بأن ما اشتملت عليه هذه الرسالة إنما هو نتاج جهدي الخاص، باستثناء ما تمت الإشارة إليه حيثما ورد، وإن هذه الرسالة ككل أو أي جزء منها لم يقدم من قبل لنيل درجة أو لقب علمي أو بحثي لدى أي مؤسسة تعليمية أو بحثية أخرى.

DECLARATION

The work provided in this thesis, unless otherwise referenced, is the researcher's own work, and has not been submitted elsewhere for any other degree or qualification

Student's name: Anas F. Al-Ghoul

Signature:

Date: 25 / 12 / 2013

اسم الطالب: أنس فهيم زياده الغول

التوقيع:

التاريخ: 25 / 12 / 2013

بسم الله الرحمن الرحيم

الجامعة الإسلامية – غزة
The Islamic University - Gaza

مكتب نائب الرئيس للبحث العلمي والدراسات العليا هاتف داخلي 1150

الرقم.....ج.س.غ/35/..... Ref

التاريخ 2013/12/25م..... Date

نتيجة الحكم على أطروحة ماجستير

بناءً على موافقة شئون البحث العلمي و الدراسات العليا بالجامعة الإسلامية بغزة على تشكيل لجنة الحكم على أطروحة الباحث/ **أنس فهيم زيادة الغول** لنيل درجة الماجستير في **كلية *الهندسة*** **قسم/ الهندسة الكهربائية–أنظمة الاتصالات** وموضوعها:

تصميم جهازي التبديل التناوبي للجيل الثاني والثالث والرابع المستخدمة في أنظمة الاتصالات الخلوية

Design of UMTS/ LTE Diplexer and DCS/ UMTS/ LTE Triplexer For Mobile Communication Systems

وبعد المناقشة العلنية التي تمت اليوم الأربعاء 22 محرم 1435هـ، الموافق 2013/12/25م الساعة الثانية عشرة ظهراً بمبنى القدس، اجتمعت لجنة الحكم على الأطروحة والمكونة من:

د. طلال فايز سكيك	مشرفاً ورئيساً	.....
د. عمار محمد أبو هدروس	مناقشاً داخلياً	.....
د. يوسف العبد حمودة	مناقشاً خارجيًا	.....

وبعد المداولة أوصت اللجنة بمنح الباحث درجة الماجستير في كلية *الهندسة*/ قسم **الهندسة الكهربائية- أنظمة الاتصالات.**

واللجنة إذ تمنحه هذه الدرجة فإنها توصيه بتقوى الله ولزوم طاعته وأن يسخر علمه في خدمة دينه ووطنه.

والله ولي التوفيق،،،

مساعد نائب الرئيس للبحث العلمي وللدراسات العليا

أ.د. فؤاد علي العاجز

P.O. Box 108, Rimal, Gaza, Palestine fax: +970 (8) 286 0800 فاكس Tel: +970 (8) 286 0700 ص.ب. 108 الرمال، غزة، فلسطين هاتف
public@iugaza.edu.ps www.iugaza.edu.ps

Abstract

The central theme of this work is the design of a compact microstrip triplexer and diplexer for mobile communication systems at base stations to work as a transceiver. The first stage includes designing individual microstrip bandpass hairpin filters. The first filter is specified to work at the Digital Cellular System (DCS) operating at 1710-1880 MHz band, whereas the second filter is specified to work at the Universal Mobile Telecommunication System (UMTS) operating at 1920-2170 MHz and the third filter is for the Long Term Evolution (LTE) system operating at 2500-2690 MHz band. The structure of each filter consists of five coupled resonators with chebyshev response. In the second stage, the individual filters are then combined together using a central transmission line that couples the energy from the common port to filters and the other way around. Two multiplexing components have been designed. The first is a diplexer for UMTS/ LTE systems, and the second component is a triplexer for DCS/ UMTS/ LTE systems. Optimization techniques available in CST simulation software such as Genetic and Nelder Mead Simplex algorithms have then been utilized to improve the performance of the whole structure of each component.

ملخص الرسالة

تقوم هذه الرسالة على أساس تصميم جهازي تبديل التناوبي ثنائي وثلاثي المجال (Diplexer and Triplexer) المستخدم في أنظمة الاتصالات اللاسلكية.

الخطوة الأولى تبدأ بتصميم مرشحات من نوع (Microstrip Hairpin). المرشح الأول تم تصميمه ليعمل ضمن نظام الهاتف الرقمي الخلوي (DCS) على النطاق الترددي (1710-1880 MHz) ويتبع للجيل الثاني، والمرشح الثاني يعمل ضمن النظام العالمي للاتصالات المتنقلة (UMTS) على النطاق الترددي (1920-2170 MHz) ويتبع للجيل الثالث، أما المرشح الأخير فيعمل ضمن شبكات التطور طويل الأجل (LTE) في النطاق الترددي (2500-2690 MHz) ويتبع لأنظمة الجيل الرابع.

يتكون كل مرشح من 5 دوائر رنين (Resonators) بينها اقتران (Coupling) للحصول على تصفية تشيبتشيف (Chebyshev filtering) من أجل ترشيح الإشارات المطلوبة. بعد ذلك يتم الجمع بين المرشحات باستخدام خط نقل مركزي (Central Transmission Line) مربوط بالمدخل الخاص بتغذية الإشارة (Input port) ليتم نقل الإشارة إلى المرشحات والعكس صحيح.

لقد تم تصميم الجهازين. الأول هو مبدل تناوبي ثنائي (Diplexer) لنظامي (UMTS/ LTE) ، أما الآخر فهو مبدل تناوبي ثلاثي (Triplexer) لأنظمة (DCS/ UMTS/ LTE) .

استخدمت تقنية التحسين للأمثل (Optimization) المتوفرة في برنامج (CST Microwave Studio) لتحسين كفاءة كلا من الجهازين.

Acknowledgements

I would like to give my particular thanks to my director of studies, Dr. Talal F. Skaik for his supervision, encouragement and guidelines throughout this research work.

The scientific support provided by the department of Electrical and Communication Engineering at the Islamic University of Gaza is gratefully acknowledged.

I would like to dedicate this work to my father's spirit, who I wished he was next to me on this occasion.

I would like to thank my mother Fathya for her support and encouragement thought all two years of studying and working towards this degree.

I would like to express gratitude to my brothers and sister, Maher, Zaher, Ahmad and Alaa whose constantly provide emotional support in many aspects.

Table of Contents

List of Acronyms vii
List of Figures ix
List of Tables xii
Chapter 1: Introduction 1

1 Introduction 1
1.1 Generations of Wireless Communication Systems 1
1.1.1 First Generation Technology (1G) 2
1.1.2 Second Generation Technology (2G – 2.75G) 3
1.1.3 Third Generation Technology (3G) 4
1.1.4 Fourth Generation Technology (4G) 5
1.2 Frequency Division Duplex (FDD) and Time Division Duplex (TDD) Systems ... 6
1.3 Multiple Access Techniques 7
1.3.1 Frequency Division Multiple Access 8
1.3.1.1 Advantages 8
1.3.1.2 Disadvantages 9
1.3.2 Time Division Multiple Access 9
1.3.2.1 Advantages 9
1.3.2.2 Disadvantages 10
1.3.3 Comparisons of FDMA, TDMA, and CDMA 11
1.4 Thesis Objective 12
1.5 Thesis Overview 12
References 13

Chapter 2: Filter Theory 14
2.1 Introduction 14
2.2 Transfer Function 14
2.3 Chebyshev Filter 14
2.3.1 Chebyshev Lowpass Prototype Filters 16

2.4 Transformation to Bandpass Filter ……. 18

2.5 Prototype k and q values ……... 20

2.6 Coupled – resonator filter ……. 21

2.6.1 Coupling Matrix for Coupled-Resonator Filters……. 22

2.6.1.1 Circuits with magnetically coupled resonator…… 23

2.6.1.2 Circuits with electrically coupled resonators ……... 26

2.6.1.3 General coupling matrix ……. 29

2.7 Optimization ……. 30

2.7.1 Cost function ……. 31

2.8 Summary …….. 32

References ……... 33

Chapter 3: Microstrip Lines and Hairpin Resonators ……... 34

3.1 Microstrip Transmission Line ……... 34

3.1.1 Waves in Microstrips …….... 34

3.1.2 Effective Dielectric Constant and Characteristic Impedance ……..... 35

3.1.3 Guided Wavelength and Propagation Constant …..…….. 35

3.1.4 Phase velocity and Electrical Length …….... 36

3.1.5 Synthesis of W/h ……..…. 36

3.2 Resonators ……... 37

3.2.1 Hairpin Resonator ……..…. 38

3.2.2 Hairpin Coupling Structures ……..…. 38

3.2.3 Unloaded quality factor ……..… 40

3.2.4 Extracting internal coupling coefficients ……..…. 41

3.2.5 Extracting external quality factor ……... 42

3.3 Summary …….. 44

References ……... 45

Chapter 4: Filter Simulation and Analysis 46

4.1 DCS Filter 46

4.2 UMTS Filter 50

4.3 LTE Filter 53

4.4 Summary 55

Chapter 5: Multiplexer Design and Simulation 57

5.1 Multiplexers 57

5.1.1 Literature Review 59

5.1.2 Multiplexer Design 63

5.1.3 Multiplexer design flowchart 64

5.2 DCS/ UMTS/ LTE Triplexer Simulation 66

5.3 UMTS/ LTE Diplexer Simulation 68

5.4 Summary 69

References 70

Chapter 6: Conclusions and Future Work 72

6.1 Conclusion 72

6.2 Future work 73

List of Acronyms

1G	First Generation
2G	Second Generation
3G	Third Generation
4G	Fourth Generation
AMPS	Advanced Mobile Phone System
AMTS	Advanced Mobile Telephone System
CSMA	Code Sense Multiple Access
DCS	Digital Cellular System
EDGE	Enhanced Data Rates for GSM Evolution
FDD	Frequency Division Duplex
FDMA	Frequency Division Multiple Access
GSM	Global System for Mobile Communications
GPRS	General Packet Radio Service
HSPA	High-Speed Packet Access
HSDPA	High-Speed Downlink Packet Access
IMTS	Improved Mobile Telephone Service
ISMA	Idle Signal Casting Multiple Access
ITU	International Telecommunication Union
IP	Internet Protocol
ISMA	Inhibit Sense Multiple Access
iDEN	Integrated Digital Enhanced Network
IMT-2000	International Mobile Telecommunications programme
LTE	Long Term Evolution
MTS	Mobile Telephone System
MMS	Multimedia Messages Service
NMT	Nordic Mobile Telephone
PDAs	Personal Digital Assistants
PRMA	Packet Reservation Multiple Access
PTT	Push To Talk
PDC	Personal Digital Cellular Technology
PRMA	Packet Reservation Multiple Access
RF	Radio Frequency

SMS	Short Message Service
S/I	Signal to Interference
TACS	Total Access Communications System
TDD	Time Division Duplex
TDMA	Time Division Multiple Access
T.L	Transmission Line
UMTS	Universal Mobile Telecommunication System

List of Figures

Figure 1.1: Evolution of wireless communication system 2
Figure 1.2: Multiple access schemes 7
Figure 1.3: FDMA/FDD channel architecture 8
Figure 1.4: TDMA/FDD channel architecture 10
Figure 1.5: TDMA frame 10
Figure 1.6: Comparison of multiple access methods 11
Figure 2.1: Attenuation characteristics for Chebyshev approach 15
Figure 2.2: Pole distribution for chebyshev response 16
Figure 2.3: Lowpass prototype filters for all-pole filters with (a) a ladder network structure and (b) its dual 16
Figure 2.4: Basic element transformation from lowpass prototype to bandpass 19
Figure 2.5: Lumped element Bandpass filter 19
Figure 2.6: Bandpass filter using (a) J-Inverters. (b) K-inverters 19
Figure 2.7: Bandpass filter circuits (a) capacitive coupling between resonators (b) inductive coupling between resonators 20
Figure 2.8: General coupled RF/microwave resonators where resonators 1 and 2 can be different in structure and have different resonant frequencies 21
Figure 2.9: Inter-coupling between coupled resonators. (a) Coupled resonator circuit with electric coupling. (b) Coupled resonator circuit with magnetic coupling. (c) Coupled resonator circuit with mixed electric and magnetic coupling 22
Figure 2.10: (a) Equivalent circuit of n-coupled resonators for loop-equation formulation. (b) Its network representation 23
Figure 2.11: Network representation for the Equivalent circuit of magnetically n-coupled resonators in N-port network 25
Figure 2.12: Network representation for the Equivalent circuit of electrically n-coupled resonators in N-port network 28
Figure 3.1: Microstrip structure 34
Figure 3.2: Electric and magnetic field lines 34
Figure 3.3: Some typical microstrip resonators: (a) lumped-element resonator; (b) quasilumped element resonator; (c) /4 line resonator (shunt series resonance); (d) /4 line resonator (shunt parallel resonance); (e) /2 line resonator; (f) ring resonator; (g) circular patch

resonator; (h) triangular patch resonator 37
Figure 3.4: Structural variations to miniaturize hairpin resonator. (a) Conventional hairpin resonator. (b) Miniaturized hairpin resonator with loaded lumped capacitor. (c) Miniaturized hairpin resonator with folded coupled lines 38
Figure 3.5: Hairpin Structures. (a) Tapped line input Hairpin filter. (b) Coupled line input Hairpin filter 39
Figure 3.6: Basic coupling structures of coupled microstrip hairpin resonators. (a) Electric coupling structure. (b) Magnetic coupling structure. (c) Mixed coupling structure 39
Figure 3.7: Two coupled hairpin resonators.....42
Figure 3.8: Amplitude response of S_{21} for two coupled resonators.....42
Figure 3.9: Tapped line external coupling.....43
Figure 3.10: Amplitude response of S21 for externally couple resonator.....43
Figure 4.1: DCS External coupling: (a) resonator design (b) S21 response.....47
Figure 4.2: DCS Internal coupling coefficients: (a) Resonator 1, 2 and 4, 5 design (b) S21 response 47
Figure 4.3: DCS Internal coupling coefficients: (a) Resonator 2, 3 and 3, 4 design (b) S21 response..... 48
Figure 4.4: DCS 5-pole hairpin filter design..... 48
Figure 4.5: DCS 5-pole hairpin filter initial response (a) S11 response (b) S21 response..... 49
Figure 4.6: DCS 5-pole hairpin filter final response (a) S11 response (b) S21 response..... 50
Figure 4.7: UMTS 5-pole hairpin filter design 51
Figure 4.8: UMTS 5-pole hairpin filter initial response (a) S11 response (b) S21 response 51
Figure 4.9: UMTS 5-pole hairpin filter final response (a) S11 response (b) S21 response 52
Figure 4.10: LTE 5-pole hairpin filter design 53
Figure 4.11: LTE 5-pole hairpin filter initial response (a) S11 response (b) S21 response 54
Figure 4.12: LTE 5-pole hairpin filter final response (a) S11 response (b) S21 response 55
Figure 5.1: conventional multiplexer with parallel-coupled bandpass filters 57
Figure 5.2: Configuration of multiplexer with a 1: *n* divider multiplexing network 58
Figure 5.3: Configuration of circulator-coupled multiplexer 58
Figure 5.4: Configuration of manifold-coupled multiplexer 59
Figure 5.5: Microstrip diplexer for UMTS and GSM 59

Figure 5.6: A compact diplexer using a square open loop 59
Figure 5.7: the diplexer using the T-shaped resonator, R1, to combine two second-order bandpass filters. Port 1 uses coupled feeding; ports 2 and 3 use tapped feed in 60
Figure 5.8: A microstrip diplexer for UMTS upload and download bands..... 60
Figure 5.9: Compact Multilayered Three-Channel Multiplexer..... 61
Figure 5.10: Microstrip triplexer for multiband applications..... 61
Figure 5.11: A frequency triplexer for UWB systems 62
Figure 5.12: Microstrip triplexer 62
Figure 5.13: Four channel filters connected to a ring manifold 63
Figure 5.14: Multiplexer design (a) UMTS/LTE Diplexer. (b) DCS/UMTS/LTE Triplexer 64
Figure 5.15: Flowchart of multiplexer design 65
Figure 5.16: Final DCS/ UMTS/ LTE Triplexer design 66
Figure 5.17: The EM simulated performance of the DCS/ UMTS/ LTE Triplexer 67
Figure 5.18: Final UMTS/ LTE Diplexer design 68
Figure 5.19: The EM simulated performance of the UMTS/ LTE Diplexer 69

List of Tables

Table 2.1: Element values for Chebyshev lowpass prototype for LAr=0.1dB ……..…. 17

Table 4.1: DCS initial and final parameters ……..…….. 50

Table 4.2: UMTS initial and final parameters ……..... 52

Table 4.3: LTE initial and final parameters ……..…… 55

Table 5.1: DCS/ UMTS/ LTE triplexer dimensions ……... 67

Table 5.2: UMTS/ LTE diplexer dimensions …….. 68

Chapter 1

Introduction

1 Introduction:

Wireless communication is the transfer of information over a distance without the use of enhanced electrical conductors or "wires". The distances involved may be short (a few meters as in television remote control) or long (thousands or of kilometers for radio communications). It encompasses various types of fixed, mobile, and portable two-way radios, cellular telephones, Personal Digital Assistants (PDAs), and wireless networking [1]. One of the most important components in wireless communication systems is the multiplexers.

Multiplexers are used to combine or separate frequency bands for transmission via a common antenna as part of a system. Its performance no doubt strongly affects system quality [2]. Input and output multiplexers include power dividers, circulators, manifold and transmission lines networks for connecting channel filters [3]. Such elements contribute to increase size and weight and also have a non negligible impact on electrical performances (insertion loss, power handling …) [3]. In order to suppress the previous elements from multiplexing networks, compact microwave multiplexers composed exclusively of coupled resonators have been introduced. This design allows a large reduction of size and weight compared to conventional microwave multiplexers. Moreover, compact multiplexers offer additional flexibility since coupling between channels may be exploited [3]. This thesis presents the design of a multiplexer for mobile communications systems. The next sections present the generations of mobile systems.

1.1 Generations of Wireless Communication Systems:

In 1895, Guglielmo Marconi opened the way for modern wireless communications by transmitting the three-dot Morse code for the letter 'S' over a distance of three kilometers using electromagnetic waves. From this beginning, wireless communications has developed into a key element of modern society. Wireless communications have some special characteristics that have motivated specialized studies. First, wireless communications relies on a scarce resource – namely, radio spectrum state. In order to foster the development of wireless communications (including telephony and

Broadcasting) those assets were privatized. Second, use of spectrum for wireless communications required the development of key complementary technologies; especially those that allowed higher frequencies to be utilized more efficiently. Because of its special nature, the efficient use of spectrum required the coordinated development of standards [4]. Figure 1.1 explains the evolution of applications in the generations of the wireless communication systems.

Figure 1.1: Evolution of wireless communication systems [5]

1.1.1 First Generation Technology (1G):

1G refers to the first generation of wireless telecommunication technology, more popularly known as cellphones. A set of wireless standards developed in the 1980's, 1G technology replaced 0G technology, which featured mobile radio telephones and such technologies as Mobile Telephone System (MTS), Advanced Mobile Telephone System (AMTS), Improved Mobile Telephone Service (IMTS), and Push to Talk (PTT)[4].

1G wireless networks used analog radio signals. Through 1G, a voice call gets modulated and transmitted between radio towers. This is done using a technique called Frequency-Division Multiple Access (FDMA) [4].

In terms of overall connection quality, it has low capacity, unreliable handoff, poor voice links, and no security at all since voice calls were played back in radio towers, making these calls susceptible to unwanted eavesdropping by third parties. However, 1G did maintain a few advantages over 2G. In comparison to 1G's analog signals, 2G's digital signals are very reliant on location and proximity. If a 2G handset made a call far away from a cell tower, the digital signal may not be strong enough to reach it. While a call made from a 1G handset had generally poorer quality than that of a 2G handset, it survived longer distances. This is due to the analog signal having a smooth curve compared to the

digital signal, which had a jagged, angular curve. As conditions worsen, the quality of a call made from a 1G handset would gradually worsen, but a call made from a 2G handset would fail completely [4].

Different 1G standards were used in various countries. One such standard is NMT (Nordic Mobile Telephone), used in Nordic countries, Eastern Europe and Russia. Others include AMPS (Advanced Mobile Phone System) used in the United States, TACS (Total Access Communications System) in the United Kingdom, C-Netz in West Germany, Radiocom 2000 in France, and RTMI in Italy [4].

1.1.2 Second Generation Technology (2G – 2.75G):

2G is the second-generation wireless telephone, which is based on digital technologies. 2G networks is basically for voice communications only, except Short Message Signals (SMS) is also available as a form of data transmission for some standards. 2G telephone technology is based on Global System for Mobile communication (GSM). 2G technologies enabled the various mobile phone networks to provide the services such as text messages, picture messages and multimedia messages (MMS). 2G technology holds sufficient security for both the sender and the receiver. All text messages are digitally encrypted. This digital encryption allows for the transfer of data in such a way that only the intended receiver can receive and read it. 2G technologies are either time division multiple access (TDMA) or code division multiple access (CDMA) [4].

TDMA allows for the division of signal into time slots. CDMA allocates each user a special code to communicate over a multiplex physical channel. Different TDMA technologies are GSM, PDC, iDEN, IS-136. CDMA technology is IS-95. GSM is the most admired standard of all the mobile technologies. GSM technology was the first one to help establish international roaming. This enabled the mobile subscribers to use their mobile phone connections in many different countries of the world's is based on digital signals, unlike 1G technologies which were used to transfer analogue signals.

The use of 2G technology requires strong digital signals to help mobile phones work. If there is no network coverage in any specific area, digital signals would be weak. 2.5G is a group of bridging technologies between 2G and 3G wireless communication. It is a digital communication allowing e-mail and simple Web browsing, in addition to voice [4].

1.1.3 Third Generation Technology (3G):

3G is the third generation of mobile phone standards and technology. It is based on the International Telecommunication Union (ITU) family of standards under the International Mobile Telecommunications programme, IMT-2000.

3G technologies enable network operators to offer users a wider range of more advanced services while achieving greater network capacity through improved spectral efficiency. Services include wide area wireless voice telephony, video calls, and broadband wireless data, all in a mobile environment. Additional features also include High Speed Packet Access (HSPA) data transmission capabilities able to deliver speeds up to 14.4 Mbit/s on the downlink and 5.8 Mbit/s on the uplink. Spectral efficiency or spectrum efficiency refers to the amount of information that can be transmitted over a given bandwidth in a specific digital communication system. HSPA is a collection of mobile telephony protocols that extend and improve the performance of existing UMTS protocols [4].

Unlike IEEE 802.11 (common names Wi-Fi or WLAN) networks, 3G networks are wide area cellular telephone networks which evolved to incorporate high-speed internet access and video telephony. IEEE 802.11 networks are short range, high-bandwidth networks primarily developed for data. Wi-Fi is the common name for a popular wireless technology used in home networks, mobile phones, video games and more. The notebook is connected to the wireless access point using a PC card wireless card. A videophone is a telephone which is capable of both audio and video duplex transmission [4].

3G technologies make use of TDMA and CDMA. 3G technologies make use of value added services like mobile television, Global Positioning System (GPS) and video conferencing. The basic feature of 3G Technology is fast data transfer rates. 3G technology is much flexible, because it is able to support the 5 major radio technologies. These radio technologies operate under CDMA, TDMA and FDMA. CDMA holds for IMT-DS (direct spread), IMT-MC (multi carrier). TDMA accounts for IMTTC (time code), IMT-SC (single carrier). FDMA has only one radio interface known as IMT-FC or frequency code. 3G is really affordable due to the agreement of industry. This agreement took place in order to increase its adoption by the users. 3G system is compatible to work with the 2G technologies. The aim of the 3G is to allow for more coverage and growth with minimum investment. There are many 3G technologies as W-CDMA, GSM EDGE, UMTS, DECT, WiMax and CDMA 2000. Enhanced data rates for GSM evolution or EDGE is termed to as a backward digital technology, because it can operate with older devices [4].

1.1.4 Fourth Generation Technology (4G):

4G refers to the fourth generation of cellular wireless standards. It is a successor to 3G and 2G families of standards. The terms of the generations generally refers to a change in the fundamental nature of the service, non-backwards compatible transmission technology and new frequency bands. 4G refers to all Internet Protocol (IP) packet-switched networks, mobile ultra-broadband (gigabit speed) access and multi-carrier transmission. Pre-4G technologies such as mobile WiMAX and first-release 3G Long Term Evolution (LTE) have been available on the market since 2006 and 2009, respectively. It is basically the extension in the 3G technology with more bandwidth and services offers in the 3G. The expectation for the 4G technology is basically the high quality audio/video streaming over end to end IP. If the IP multimedia sub-system movement achieves what it going to do, nothing of this possibly will matter [4].

WiMAX or mobile structural design will become progressively more translucent, and therefore the acceptance of several architectures by a particular network operator ever more common. Some of the companies trying 4G communication at 100 Mbps for mobile users and up to 1 Gbps over fixed stations [4].

1.2 Frequency Division Duplex (FDD) and Time Division Duplex (TDD) System:

Many cellular systems (such as AMP, GSM, etc.) use frequency division duplex (FDD) in which the transmitter and receiver operate simultaneously on different frequencies. Separation is provided between the downlink and uplink channels to avoid the transmitter causing self interference to its receiver [6].

A cellular system can be designed to use one frequency band by using time division duplex (TDD). In TDD a bidirectional flow of information is achieved using the simplex-type scheme by automatically alternating in time the direction of transmission on a single frequency. At best TDD can only provide a quasi-simultaneous bidirectional flow, since one direction must be off while the other is using the frequency. However, with a high enough transmission rate on the channel, the off time is not noticeable during conversations, and with a digital speech system, the only effect is a very short delay [6].

The amount of spectrum required for both FDD and TDD is the same. The difference lies in the use of two bands of spectrum separated by the required bandwidth for FDD, whereas TDD requires only one band of frequencies but twice the bandwidth. It may be easier to

find a single band of unassigned frequencies than finding two bands separated by the required bandwidth [6].

With TDD systems, the transmit time slot and the receiver time slot of the subscriber unit occur at different times. With the use of a simple RF switch in the subscriber unit, the antenna can be connected to the transmitter when a transmit burst is required (thus disconnecting the receiver from the antenna) and to the receiver for the incoming signal. The RF switch thus performs the function of the duplexer, but is less complex, smaller in size, and less costly. TDD uses a burst mode scheme like TDMA and therefore also does not require a duplexer. Since the bandwidth of a TDD channel is twice that of a transmitter and receiver in an FDD system, RF filters in all the transmitters and receivers for TDD systems must be designed to cover twice the bandwidth of FDD system filters [6].

1.3 Multiple Access Techniques:

Multiplexing deals with the division of the resources to create multiple channels. Multiplexing can create channels in frequency, time, etc., and the corresponding terms are then frequency division multiplexing (FDM), time division multiplexing (TDM), etc. Since the amount of spectrum available is limited, we need to find ways to allow multiple users to share the available spectrum simultaneously. Shared access is used to implement a multiple access scheme when access by many users to a channel is required. For example, one can create multiple channels using TDM, but each of these channels can be accessed by a group of users using the ALOHA multiple access scheme. The multiple access schemes can be either reservation-based or random [6].

Multiple access schemes can be classified as reservation-based multiple access (e.g., FDMA, TDMA, CDMA) and random multiple access (e.g., ALOHA, CSMA), see Figure1.2. If data traffic is continuous and a small transmission delay is required (for example in voice communication) reservation-based multiple access is used [6].

In many wireless systems for voice communication, the control channel is based on random multiple-access and the communication channel is based on FDMA, TDMA, or CDMA. The reservation-based multiple access technique has a disadvantage in that once the channel is assigned, it remains idle if the user has nothing to transmit, while other users may have data waiting to be transmitted. This problem is critical when data generation is random and has a high peak-rate to average-rate ratio. In this situation, random multiple-access is more efficient, because a communication channel is shared by many users and

users transmit their data in a random or partially coordinated fashion. ALOHA and carrier sense multiple access (CSMA) are examples of random multiple access. If the data arrives in a random manner, and the data length is large, then random multiple access combined with a reservation protocol will perform better than both random and reservation based schemes [6].

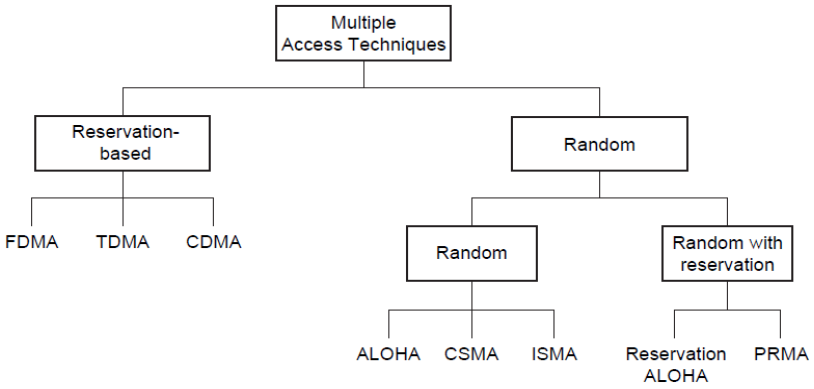

Figure 1.2: Multiple access schemes.

1.3.1 Frequency Division Multiple Access:

The FDMA is the simplest scheme used to provide multiple-access. It separates different users by assigning a different carrier frequency, see Figure 1.3. Multiple users are isolated using bandpass filters. In FDMA, signals from various users are assigned different frequencies, just as in an analog system. Frequency guard bands are provided between adjacent signal spectra to minimize crosstalk between adjacent channels. The advantages and disadvantages of FDMA with respect to TDMA or CDMA are [6]:

1.3.1.1: Advantages:

1. Capacity can be increased by reducing the information bit rate and using an efficient digital speech coding scheme.
2. Technological advances required for implementation are simple. A system can be configured so that improvements in terms of a lower bit rate speech coding could be easily incorporated.
3. Hardware simplicity, because multiple users are isolated by employing simple bandpass filters.

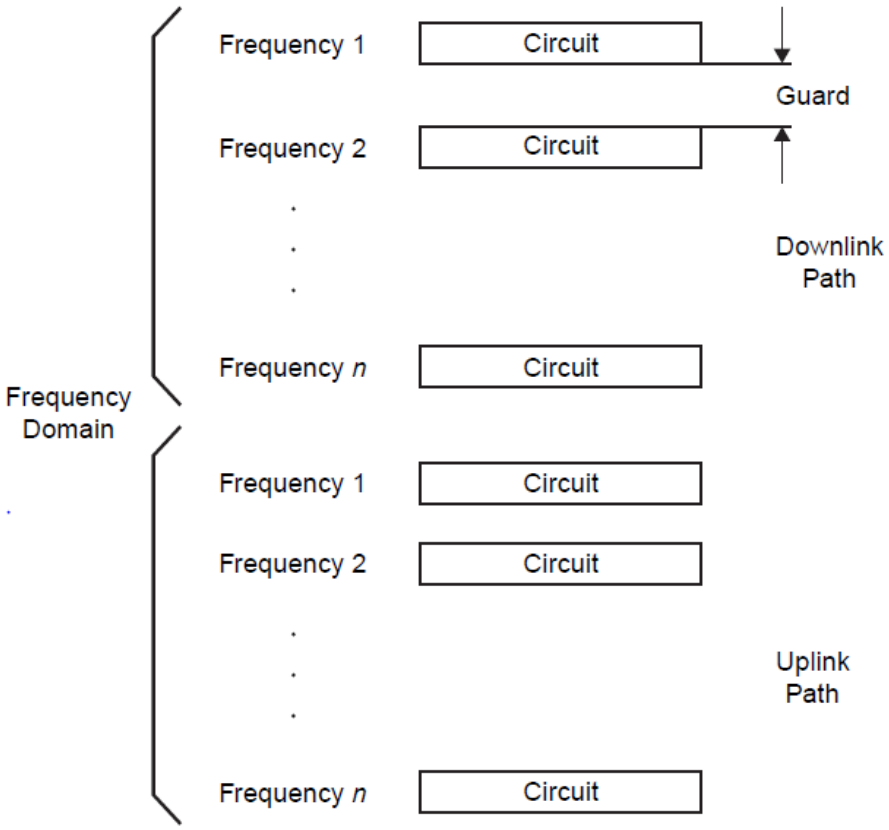

Figure 1.3: FDMA/FDD channel architecture [6].

1.3.1.2 Disadvantages:

1. The system architecture based on FDMA was implemented in first generation analog systems such as advanced mobile phone system (AMPS). The improvement in capacity depends on operation at a reduced signal-to-interference (S/I) ratio. But the narrowband digital approach gives only limited advantages in this regard so that modest capacity improvements could be expected from the allocated spectrum.

2. The maximum bit-rate per channel is fixed and small, inhibiting the flexibility in bit-rate capability that may be a requirement for computer file transfer in some applications in the future.

3. Inefficient use of spectrum, in FDMA if a channel is not in use; it remains idle and cannot be used to enhance the system capacity.

1.3.2 Time Division Multiple Access:

In a TDMA system, each user uses the whole channel bandwidth for a fraction of time, see figure 1.4, compared to an FDMA system where a single user occupies the channel bandwidth for the entire duration. In a TDMA system, time is divided into equal time

intervals, called slots. User data is transmitted in the slots. Several slots make up a frame. Guard times are used between each user's transmissions to minimize crosstalk between channels, see figure 1.5. Each user is assigned a frequency and a time slot to transmit data. The data is transmitted via a radio carrier from a base station to several active mobiles in the downlink. In the reverse direction (uplink), transmission from mobiles to base stations is time-sequenced and synchronized on a common frequency for TDMA. The preamble carries the address and synchronization information that both base station and mobile stations use for identification, the advantages and disadvantages of TDMA are [6]:

1.3.2.1 Advantages:

1. TDMA permits a flexible bit rate.

2. TDMA offers the opportunity for frame-by-frame monitoring of signal strength/bit error rates to enable either mobiles or base stations to initiate and execute handoffs.

3. TDMA, when used exclusively and not with FDMA, utilizes bandwidth more efficiently because no frequency guard band is required between channels.

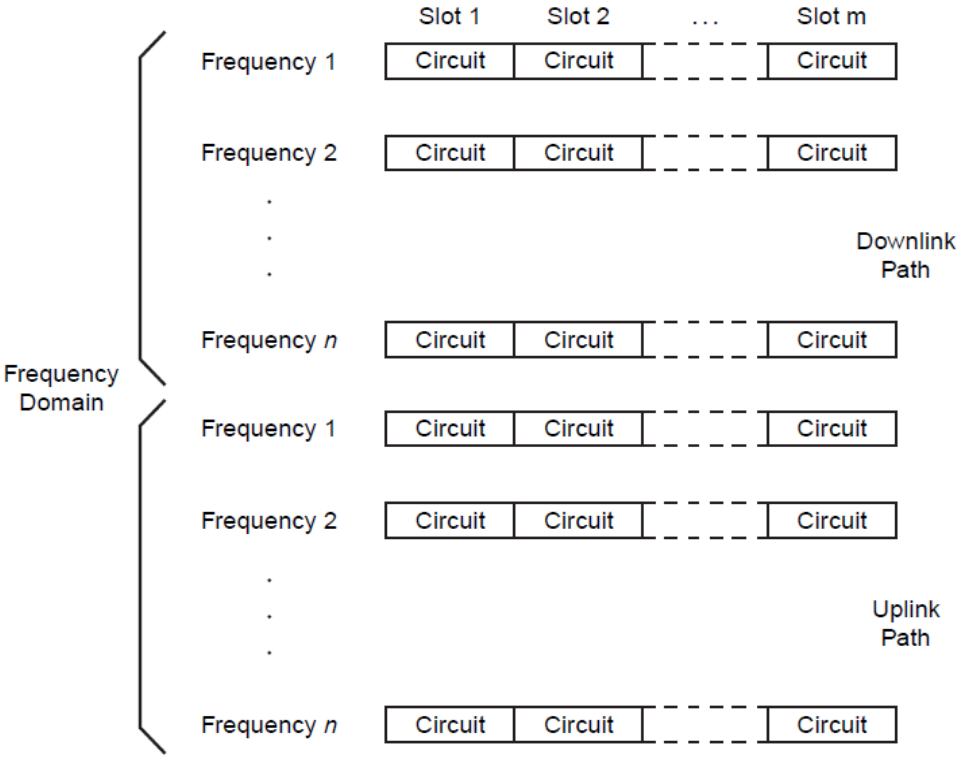

Figure 1.4: TDMA/FDD channel architecture [6].

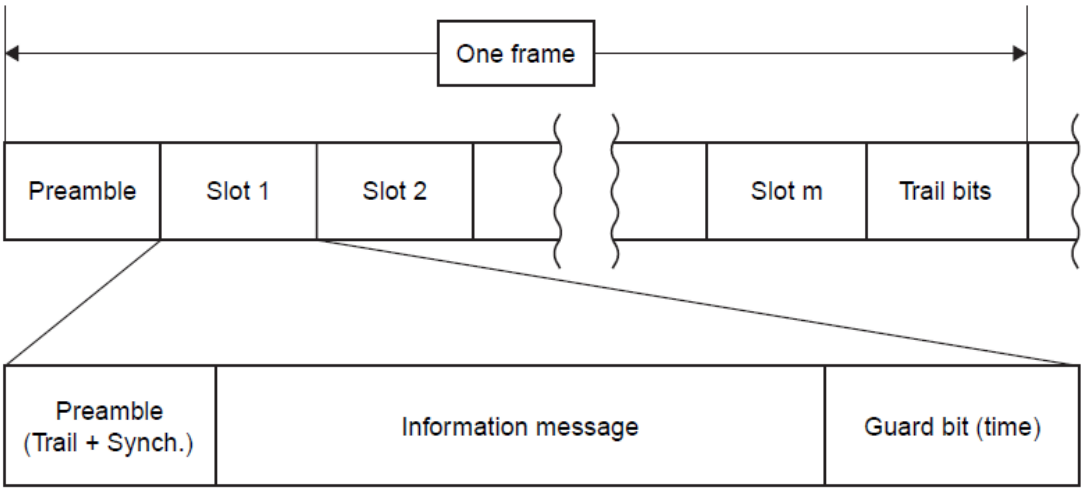

Figure 1.5: TDMA frame [6].

1.3.2.2 Disadvantages:

1. For mobiles and particularly for hand-sets, TDMA on the uplink demands high peak power in transmit mode, which shortens battery life.
2. TDMA requires a substantial amount of signal processing for matched filtering and correlation detection for synchronizing with a time slot.
3. TDMA requires synchronization. If the time slot synchronization is lost, the channels may collide with each other.

1.3.3 Comparisons of FDMA, TDMA, and CDMA:

The primary advantage of CDMA is its ability to tolerate a fair amount of interfering signals compared to FDMA and TDMA that typically cannot tolerate any such interference (Figure 1.6). As a result of the interference tolerance of CDMA, the problems of frequency band assignment and adjacent cell interference are greatly simplified. Also, flexibility in system design and deployment are significantly improved since interference to others is not a problem. On the other hand, FDMA and TDMA radios must be carefully assigned a frequency or time slot to assure that there is no interference with other similar radios [6].

With CDMA, adjacent microcells share the same frequencies whereas with FDMA/TDMA it is not feasible for adjacent microcells to share the same frequencies because of interference. In both FDMA and TDMA systems, a time-consuming frequency planning task is required whenever a network changes, whereas no such frequency planning is needed for a CDMA network since each cell uses the same frequencies [6].

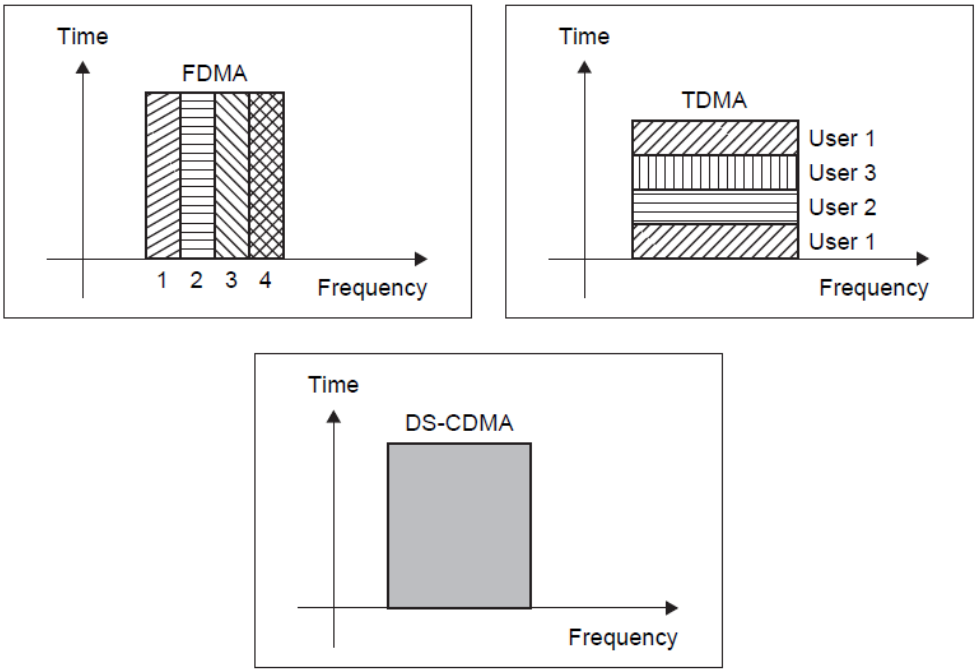

Figure 1.6: Comparison of multiple access methods.

1.4 Thesis Objective:

Microwave multiplexing networks are widely used in wireless communications systems. The frequency spectrums can be split into a number of smaller frequency bands or Radio Frequency (RF) channels using input multiplexers. Output multiplexers combine several narrowband channels into a single wideband composite signal for transmission. The performances of channel filters, such as the insertion loss and rejection between channels, are extremely critical [2].

A typical multiplexer design involves design and optimization. In the design process, the channel filters are prepared to meet the specifications with the corresponding coupling matrices synthesized, then the filters are combined together using a power distribution network such as transmission lines, manifolds, circulators and power dividers.

The proposed work here is to analyze and design a microstrip multiplexer for mobile base stations. Two devices are designed; the first is a diplexer supporting UMTS and LTE systems, and the second device is a triplexer supporting DCS, UMTS, and LTE mobile communication systems. The specification of each particular channel has been introduced early in this chapter.

1.5 Thesis Overview:

In this chapter we explained the history of wireless communication and the evolution of its generations. We explained the importance of multiplexer components for communication systems.

The next chapter discusses the bandpass filter design procedure, chebyshev filters will be explained.

Chapter 3 explains the microstrip lines and their design equations. The hairpin resonators design will also be discussed. The theory of coupling, the calculation of coupling coefficients between two resonators, and the calculation of external coupling coefficients will also be presented in chapter 3.

Chapter 4 presents the design of each channel filter using microstrip technology. The insertion and return loss of each filter will be shown from simulation results.

Chapter 5 explains the design procedure for the DCS (GSM 1800)/ UMTS/ LTE triplexer and UMTS/ LTE diplexer.

The final chapter provides summary and conclusions drawn from this work.

References:

[1] M. Bhalla and A. Bhalla, "Generations of Mobile Wireless Technology: A Survey," International Journal of Computer Applications, Vol.5– No.4, August 2010.

[2] S. Li, "Effective Design of Multiplexing Networks for Applications in Communications Satellites," MSc dissertation, Univ. of Ontario Institute of Technology, Engineering and Applied Science Dept., Canada, 2011.

[3] S. Bila, H. Ezzeddine, D. Baillargeat, S. Verdeyme and F. Seyfert, "Advanced Design of Microwave Filters and Multiplexers," Proceedings of the Asia-Pacific Microwave Conference, 2011.

[4] G. Kaur, J. Birla, J. Ahlawat," Generations of Wireless Technology," IJCSMS International Journal of Computer Science and Management Studies, Vol.11, Issue 02, Aug 2011, pp. 2231-5268.

[5] Maximizing Border website, [Online]. Available: http://shishireahmed.blogspot.com/2012/09/long-term-evolution-lte.html

[6] V. Garg, Wireless Communications and Networking. San Francisco, 2007.

Chapter 2

Filter Theory

In this chapter we will discuss the theoretical procedure for design of the microstrip filters.

2.1 Introduction:

Bandpass filters play a significant role in wireless communication systems. Transmitted and received signals have to be filtered at a certain center frequency with a specific bandwidth [1]. The rapid growth in commercial microwave communication systems had been developed. Hence microstrip technology play important role in many RF or Microwave applications. Emerging applications such as wireless communications continue to challenge RF/Microwave filters with requirements of higher performance, smaller size, lighter weight and lower cost [2].

2.2 Transfer Function:

In Radio Frequency (RF) applications, for defining transfer function we use the scattering parameter S_{21}. In many applications we use instead the magnitude of S_{21}, the quadrate of S_{21} is preferred [1],

$$|S_{21}(j\Omega)|^2 = \frac{1}{1+\varepsilon^2 F_n^2(\Omega)} \tag{2.1}$$

where, ε is the ripple constant, $F_n(\Omega)$ filter function and Ω is frequency variable. If the transfer function is given, the insertion loss response of the filter can calculated by

$$L_A(\Omega) = 10\log\frac{1}{|S_{21}(j\Omega)|^2}\,dB \tag{2.2}$$

For lossless conditions, the return loss can be found by

$$L_R = 10\log[1 - |S_{21}(j\Omega)|^2]\,dB \tag{2.3}$$

2.3 Chebyshev Filter:

In practical implementation, the specification for losses in pass region can normally be higher than zero. Chebyshev approach exploits this not so strictly given specification values. It can be 0.01 dB, or 0.1 dB, or even higher values. The Chebyshev approach thereby shows certain ripples in the pass region, this can lead to better (higher) slope in the

stop region. Figure 2.1 shows the attenuation characteristics for lowpass filter based on Chebyshev approach. The quadrate of the magnitude of the transfer function with Chebyshev approach is given by [1]:

$$|S_{21}(j\Omega)|^2 = \frac{1}{1+\varepsilon^2 T_n^2(\Omega)} \tag{2.4}$$

$T_n(\Omega)$ is the first kind chebyshev function of order n, defined by [3]:

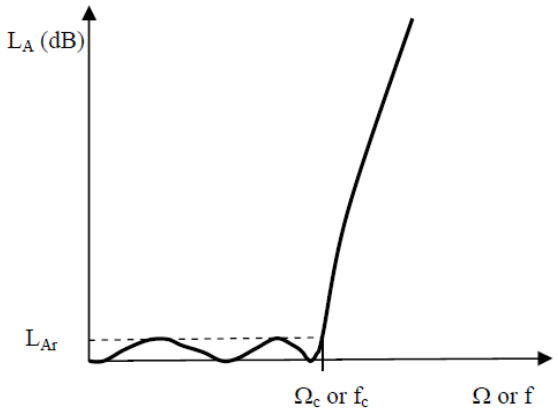

Figure 2.1: Attenuation characteristics for Chebyshev approach [1].

$$T_n(\Omega) = \begin{cases} \cos(n\cos^{-1}\Omega), & |\Omega| \le 1 \\ \cosh(n\cosh^{-1}\Omega), & |\Omega| \ge 1 \end{cases} \tag{2.5}$$

The chebyshev filter has the following general rational transfer function [3]:

$$S_{21}(p) = \frac{\prod_{i=1}^{n}[\eta^2+\sin^2(i\pi/n)]^{\frac{1}{2}}}{\prod_{i=1}^{n}(p+p_i)} \tag{2.6}$$

with

$$p_i = j\cos\left[\sin^{-1} j\eta + \frac{(2i-1)\pi}{2n}\right] \tag{2.7}$$

$$\eta = \sinh\left(\frac{1}{h}\sinh^{-1}\frac{1}{\varepsilon}\right) \tag{2.8}$$

All the transmission zeros of the transfer function are located at infinity. Therefore, chebyshev filters are known as all pole filters. The poles of the chebyshev filter are located on an ellipse in the left half plane with major axis of size $\sqrt{1+\eta^2}$ on the jΩ-axis and minor axis of size η on the σ-axis [3]. For a 5^{th} order chebyshev filter, the pole distribution is shown in figure 2.2 [3]. Lowpass prototype filters generally have the element values normalized to make the source resistance equal to one ($g_0 = 1$), and the angular cutoff

frequency $\Omega_c = 1$ (rad/sec). Generally, n-pole lowpass prototype for Butterworth, Chebyshev and Gaussian responses have two forms that give the same response. The forms are dual from each other and are shown in figure 2.3.

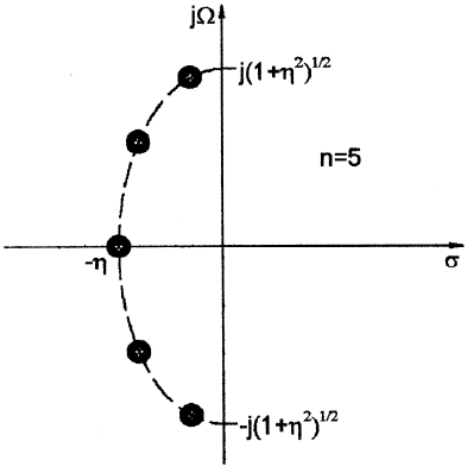

Figure 2.2: Pole distribution for chebyshev response [3].

where g_i^s for $i = 1$ to n in figure 2.2 represents series inductor or shunt capacitor, where n is the order of the filter and represents the number of reactive elements in the prototype structure. g_0 is known as the source resistance or inductance, whereas g_{n+1} is defined as the load resistance or the load conductance.

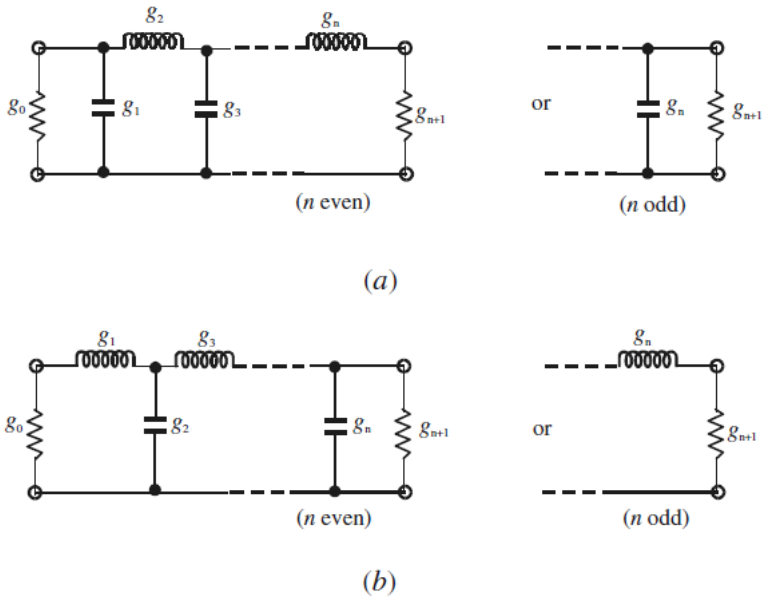

Figure 2.3: Lowpass prototype filters for all-pole filters with (a) a ladder network structure, and (b) its dual.

2.3 Chebyshev Lowpass Prototype Filters:

The component values can be calculated with the following rules [1]

$$g_0 = 1, \tag{2.9}$$

$$g_1 = \frac{2}{\gamma}\sin\left(\frac{\pi}{2n}\right), \tag{2.10}$$

$$g_i = \frac{1}{g_{i-1}} \frac{4\sin\left(\frac{(2i-1)\pi}{2n}\right)\sin\left(\frac{(2i-3)\pi}{2n}\right)}{\gamma^2 + \sin^2\left(\frac{(i-1)\pi}{n}\right)} \sin\left(\frac{(2i-1)\pi}{2n}\right), \tag{2.11}$$

For $i = 2$ to n

$$g_{n+1} = \begin{cases} 1 & for\ odd\ n \\ \coth^2\left(\frac{\beta}{4}\right) & for\ even\ n, \end{cases} \tag{2.12}$$

where,

$$\beta = \ln\left[\coth\left(\frac{L_{A,r}}{17.37}\right)\right] \quad \text{and} \quad \gamma = \sinh\left(\frac{\beta}{2n}\right).$$

The element values for chebyshev lowpass prototype network for passband ripple $L_{Ar} = 0.1$ dB are given in Table 2.1 for filter order of $n = 1$ to 9, $g_0 = 1$, and $\Omega_c = 1$. The order of the filter is determined according to the required specifications; such as the minimum stopband attenuation L_{As} dB at $\Omega = \Omega_s$ for $\Omega_s > 1$ and passband ripple L_{Ar} dB. The order of Chebyshev lowpass prototype response is calculated by [3]:

Table 2.1: Element values for Chebyshev lowpass prototype for $L_{Ar} = 0.1$ dB.

n	g_1	g_2	g_3	g_4	g_5	g_6	g_7	g_8	g_9	g_{10}
1	0.3052	1.0								
2	0.8431	0.6220	1.3554							
3	1.0316	1.1474	1.0316	1.0						
4	1.1088	1.3062	1.7704	0.8181	1.3554					
5	1.1468	1.3712	1.9750	1.3712	1.1468	1.0				
6	1.1681	1.4040	2.0562	1.5171	1.9029	0.8618	1.3554			
7	1.1812	1.4228	2.0967	1.5734	2.0967	1.4228	1.1812	1.0		
8	1.1898	1.4346	2.1199	1.6010	2.1700	1.5641	1.9445	0.8778	1.3554	
9	1.1957	1.4426	2.1346	1.6167	2.2054	1.6167	2.1346	1.4426	1.1957	1.0

$$\mathrm{n} \geq \frac{\cosh^{-1}\sqrt{\frac{10^{0.1L_{As}}-1}{10^{0.1L_{Ar}}-1}}}{\cosh^{-1}\Omega_s} \tag{2.13}$$

Impedance scaling and frequency transformation are applied to the lowpass prototype structure. Impedance scaling adjusts the value of g_0 to the value of source impedance Z_0, and hence removes the normalization of $g_0 = 1$. Impedance scaling factor γ_0 is defined as

$\gamma_0 = Z_0/g_0$ for g_0 being resistance, and $\gamma_0 = g_0/Y_0$ for g_0 being conductance. The impedance scaling is applied on the filter network as follows [3]:

$L \longrightarrow \gamma_0 L \qquad C \longrightarrow C/\gamma_0 \qquad R \longrightarrow R\gamma_0 \qquad G \longrightarrow G\gamma_0$

2.4 Transformation to Bandpass Filter:

The previous observation was done for lowpass implementation. A transformation to bandpass is needed for getting bandpass characteristics. In the transformation, the component L will be converted to serial combinations of L_s and C_s, whereas the component C becomes parallel combination of L_P and C_P. With the cut-off frequencies w_1 and w_2 as lower and upper boundary, we can calculate the center frequency and the fractional bandwidth as follows [1]:

$\omega_0 = \sqrt{\omega_1 \omega_2}$ and $FBW = \frac{\omega_2 - \omega_1}{\omega_0}$

and the values for the new components are,

$$L_s = \left(\frac{1}{FBW.\omega_0}\right) Z_0.g, \tag{2.14}$$

$$C_s = \left(\frac{FBW}{\omega_0}\right) \frac{1}{Z_0.g}, \tag{2.15}$$

for the serial combination, and

$$C_p = \left(\frac{1}{FBW.\omega_0}\right) \frac{g}{Z_0}, \tag{2.16}$$

$$L_p = \left(\frac{FBW}{\omega_0}\right) \frac{Z_0}{g}, \tag{2.17}$$

for the parallel combination.

where Z_0 is the value of the load impedance, normally set to 50 Ω. The lowpass prototype to bandpass element transformation is shown in figure 2.4 [3]. The transformation of the lowpass prototype of the circuit shown in figure 2.3 to bandpass is shown in figure 2.5 [4]. The J and K inverters are used to convert the previous circuit to an equivalent form that is more suitable for implementation. The use of J inverters makes the circuit with only parallel resonators as shown in figure 2.6(a), whereas the use of k inverters makes the circuit with only series resonators as shown in figure 2.6(b). The J and K inverters are

called immittance inverters, and there are various forms that operate as immitance invertors [4].

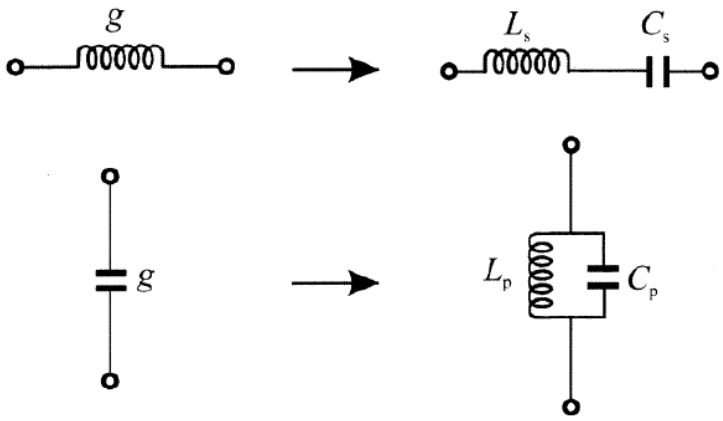

Figure 2.4: Basic element transformation from lowpass prototype to bandpass

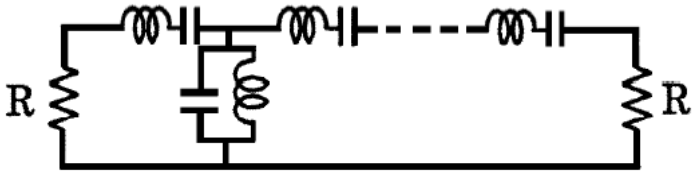

Figure 2.5: Lumped element Bandpass filter.

The J inverters in figure 2.6(a) can be replaced by π-type capacitors and the resulting circuit will contain shunt resonators connected by series capacitors as shown in figure 2.7(a), and the capacitors represent capacitive coupling coefficients between adjacent resonators. Similarly, the K inverters can be replaced by inductors and the resulting circuit will contain series resonators connected by parallel inductors as shown in figure 2.7(b), and the inductors represent inductive coupling coefficients between adjacent resonators [4].

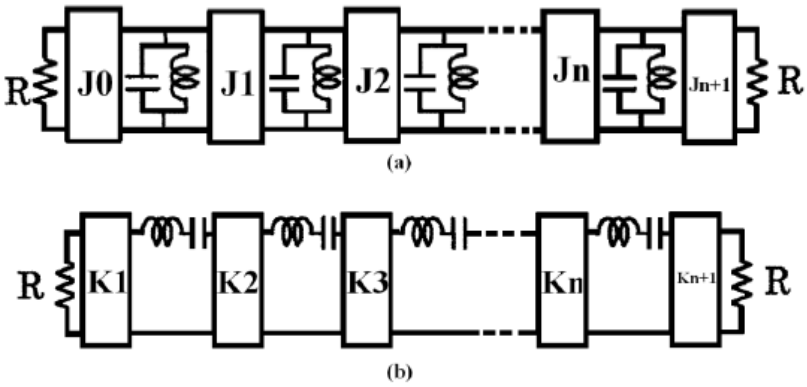

Figure 2.6: Bandpass filter using (a) J-Inverters. (b) K-inverters.

The lumped LC resonators shown in figure 2.7 can be replaced by distributed circuits such as microwave resonators, but this is convenient only for narrow band filters because the reactances or susceptances of the microwave resonators are approximately equal to those of lumped elements only near resonance, which is a small frequency range [4].

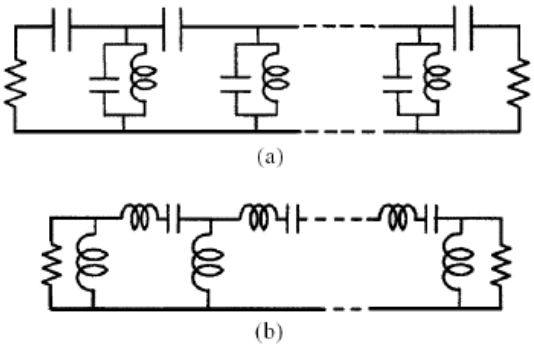

Figure 2.7: Bandpass filter circuits (a) capacitive coupling between resonators (b) inductive coupling between resonators.

2.5 Prototype k and q values:

Define k and q as prototype values, where k represents coupling between two resonators, and q represents the external coupling. The q prototype values can be derived from prototype g vales as follows [4]:

$$q_1 = g_0 g_1 \,, \tag{2.18}$$

$$\mathrm{q_n} = \begin{cases} \mathrm{g_n g_{n+1}}, & for\ n\ even, \\ \frac{\mathrm{g_n}}{\mathrm{g_{n+1}}}, & for\ n\ odd, \end{cases} \tag{2.19}$$

where q_1 and q_n are related to the input and output coupling respectively. The k prototype value is derived from prototype g values as follows:

$$k_{i,i+1} = \frac{1}{\sqrt{g_i g_{i+1}}} \quad for\ i = 1\ to\ n-1, \tag{2.20}$$

Both k and q are normalized to a unity fractional bandwidth ($FBW = 1$), the actual values for k and q are denormalized as follows:

$$K_{i,j} = K_{i,j} \frac{BW}{f_0} \,, \tag{2.21}$$

$$Q_1 = q_1 \frac{f_0}{BW}, \qquad and \qquad Q_n = q_n \frac{f_0}{BW} \,, \tag{2.22}$$

where f_0 is the centre frequency of the bandpass filter and BW is the absolute bandwidth. Q is known as the external quality factor, and the external coupling coefficient is equal to $K_e = 1/Q$. The design of bandpass filters is straightforward and is based on the g prototype values.

2.6 Coupled – resonator filter:

There is a general technique for designing coupled resonator filters that can be applied to the design of microstrip filters. This design method is based on coupling coefficients of intercoupled resonators and the external quality factors of the input and output resonators [3]. In general, the coupling coefficient of coupled RF/microwave resonators, which can be different in structure and can have different self-resonant frequencies (see Figure 2.8), may be defined on the basis of the ratio of coupled energy to stored energy [3], i.e.,

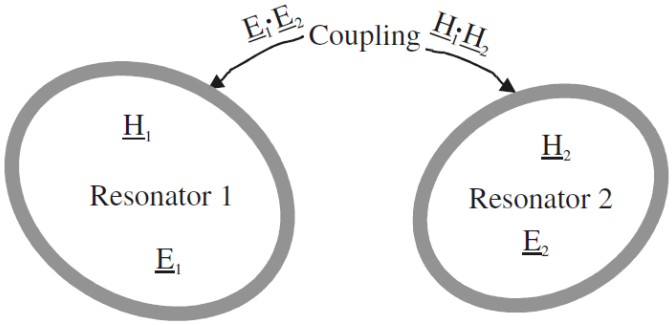

Figure 2.8: General coupled RF/microwave resonators where resonators 1 and 2 can be different in structure and have different resonant frequencies.

$$k = \frac{\iiint \varepsilon \underline{E}_1 . \underline{E}_2 \, dv}{\sqrt{\iiint \varepsilon |\underline{E}_1|^2 \, dv \times \iiint \varepsilon |\underline{E}_2|^2 dv}} + \frac{\iiint \mu \underline{H}_1 . \underline{H}_2 \, dv}{\sqrt{\iiint \mu |\underline{H}_1|^2 \, dv \times \iiint \mu |\underline{H}_2|^2 dv}}, \qquad (2.22)$$

where $\underline{E}$ and $\underline{H}$ represent the electric and magnetic field vectors, respectively.

The first term on the right-hand side represents the electric coupling and the second term the magnetic coupling, a positive sign would imply that the coupling enhances the stored energy of uncoupled resonators, whereas a negative sign would indicate a reduction. Therefore, the electric and magnetic couplings could either have the same effect if they have the same sign, or have the opposite effect if their signs are opposite. Obviously, the direct evaluation of coupling coefficient from equation (2.22) requires the knowledge of

the field distributions and needs to perform the space integrals. This would never be an easy task unless analytical solutions of the fields exist [3].

On the other hand, it would be much easier to find some characteristic frequencies that are associated with the couplings. The coupling coefficient can then be determined if the relationships between the coupling coefficient and the characteristic frequencies are established. In what follows the formulation of such relationships derived [3].

Before processing further, it might be worth pointing out that although the following derivations are based on lumped element circuit models, the outcomes are also valid for distributed element coupled structures on a narrow-band basis [3]. Figure 2.9 shows the different types of coupling which could be electric coupling, magnetic coupling or mixed coupling.

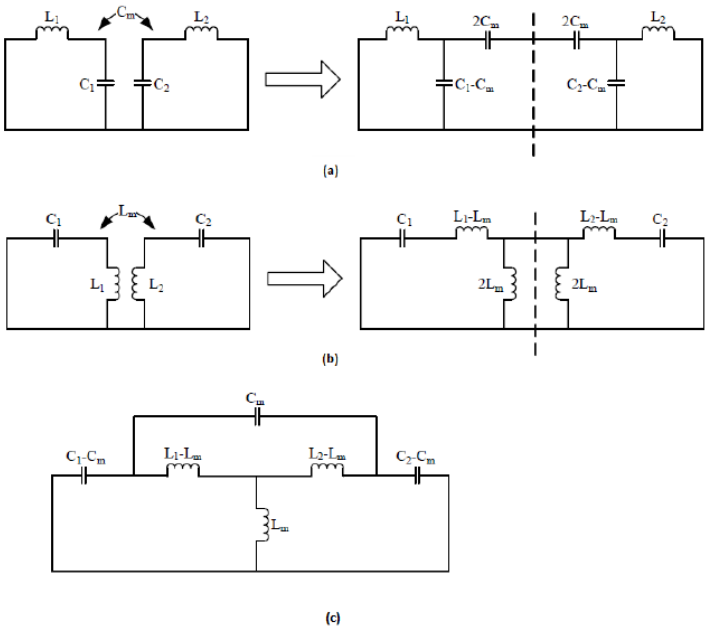

Figure 2.9: Inter-coupling between coupled resonators. (a) Coupled resonator circuit with electric coupling. (b) Coupled resonator circuit with magnetic coupling. (c) Coupled resonator circuit with mixed electric and magnetic coupling.

2.6.1 Coupling Matrix For Coupled-Resonator Filters:

Coupled resonator circuits are the basis for the design of bandpass microwave filters. The general coupling matrix of n-coupled resonators and a detailed derivation of the general coupling matrix and its relation to the scattering parameters are presented in the next sections. In a coupled resonator circuit, energy may be coupled between adjacent resonators by a magnetic field or an electric field or both as shown in figure 2.9 [3]. The coupling matrix can be derived from the equivalent circuit by formulation of impedance matrix for magnetically coupled resonators or admittance matrix for electrically coupled

resonators. This approach has been used to derive the coupling matrix of an n-coupled resonators circuit. Magnetic coupling and Electric coupling will be considered separately and later a solution will be generalized for both types of couplings [3].

In the case of magnetically coupled resonators, as shown in figure 2.10 using Kirchhoff's voltage law, the loop equations are derived from the equivalent circuit, and represented in impedance matrix form. Similarly, for electrically coupled resonators, using Kirchhoff's current law, node equations are derived from the equivalent circuit, and represented in admittance matrix form [3].

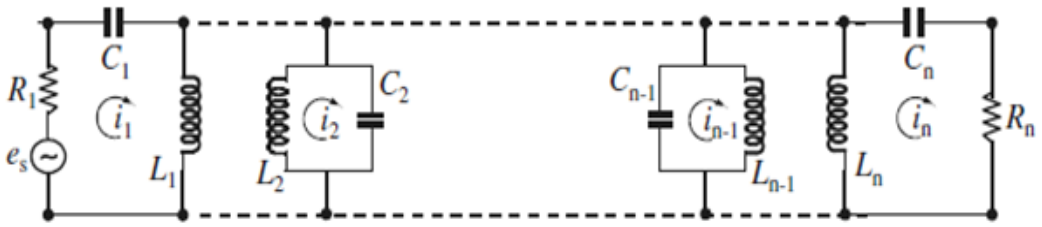

Figure 2.10: Equivalent circuit of n-coupled resonators for loop-equation formulation [3].

2.6.1.1 Circuits with magnetically coupled resonators:

Suppose only magnetic coupling between adjacent resonators, the equivalent circuit of magnetically coupled n-resonators with multiple ports is shown in Figure 2.10, where i represents loop current, L, C denote the inductance and capacitance, and R denotes the resistance (represents a port). It is assumed that the signal source is connected to resonator 1. It is also assumed that the coupling exists between all the resonators [3].

Using Kirchhoff's voltage law, the loop equations are derived as follows,

$$\left(R_1 + jwL_1 + \frac{1}{jwC_1}\right) i_1 - jwL_{12} i_2 \ldots - jwL_{1n} i_n = e_s,$$

$$-jwL_{12} i_1 + \left(jwL_2 + \frac{1}{jwC_2}\right) i_2 \ldots - jwL_{2n} i_n = 0, \qquad (2.23)$$

.

$$-jwL_{n1} i_1 - jwL_{n2} i_2 + \cdots + \left(R_n + jwL_n + \frac{1}{jwC_n}\right) i_n = 0,$$

where $L_{ab} = L_{ba}$ denotes the mutual inductance between resonators a and b. The matrix form representation of these equations is as follows,

$$\begin{bmatrix} R_1 + jwL_1 + \frac{1}{jwC_1} & -jwL_{12} & -jwL_{1n} \\ -jwL_{21} & jwL_2 + \frac{1}{jwC_2} & -jwL_{2n} \\ -jwL_{n1} & -jwL_{n2} & R_n + jwL_n + \frac{1}{jwC_n} \end{bmatrix} \begin{bmatrix} i_1 \\ \vdots \\ i_n \end{bmatrix} = \begin{bmatrix} e_s \\ 0 \\ 0 \end{bmatrix}, \quad (2.24)$$

or equivalently $[Z].[i] = [e]$, where $[Z]$ is the impedance matrix. Assuming all resonators are synchronized at the same resonant frequency $\omega_0 = 1/\sqrt{LC}$, where $L = L_1 = L_2 = \cdots L_n$ and $C = C_1 = C_2 = \cdots C_n$, the impedance matrix $[Z]$ can be expressed by $[Z] = \omega_0 L.FBW.\overline{[Z]}$ where FBW is the fractional bandwidth, and $\overline{[Z]}$ is normalized impedance matrix, given by [3],

$$\overline{[Z]} = \begin{bmatrix} \frac{R_1}{\omega_0 L(FBW)} + P & -\frac{jwL_{12}}{\omega_0 L}\frac{1}{FBW} & \cdots & -\frac{jwL_{1n}}{\omega_0 L}\frac{1}{FBW} \\ -\frac{jwL_{21}}{\omega_0 L}\frac{1}{FBW} & P & \cdots & -\frac{jwL_{2n}}{\omega_0 L}\frac{1}{FBW} \\ \vdots & \vdots & & \vdots \\ -\frac{jwL_{n1}}{\omega_0 L}\frac{1}{FBW} & -\frac{jwL_{n2}}{\omega_0 L}\frac{1}{FBW} & \cdots & \frac{R_n}{\omega_0 L(FBW)} + P \end{bmatrix}, \quad (2.25)$$

with $P = \frac{j}{FBW}\left(\frac{\omega}{\omega_0} - \frac{\omega_0}{\omega}\right)$ is the complex lowpass frequency variable.

Defining the external quality factor for resonator i as $Q_{ei} = \omega_0 L/R_i$, and the coupling coefficient as $M_{ij} = L_{ij}/L$, and assuming $\omega/\omega_0 \approx 1$ for narrow band approximation, $\overline{[Z]}$ is simplified to,

$$\overline{[Z]} = \begin{bmatrix} \frac{1}{q_{e1}} + P & -jm_{12} & \cdots & -jm_{1n} \\ -jm_{21} & P & \ldots & -jm_{2n} \\ -jm_{n1} & -jm_{n2} & \cdots & \frac{1}{q_{en}} + P \end{bmatrix} \quad (2.26)$$

where q_{ei} is the scaled external quality factor ($q_{ei} = Q_{ei}.FBW$) and m_{ij} is the normalized coupling coefficient ($m_{ij} = M_{ij}.FBW$). The network representation for the circuit in Figure 2.11, considering only two-ports, is shown in Figure 2.10, a_1, b_1, a_2, b_2 where are the wave variables, V_1, I_1, V_2, I_2 are the voltage and current variables, it can be identified that $I_1 = i_1, I_2 = -i_n$ and $V_1 = e_s - i_1 R_1$ then we have,

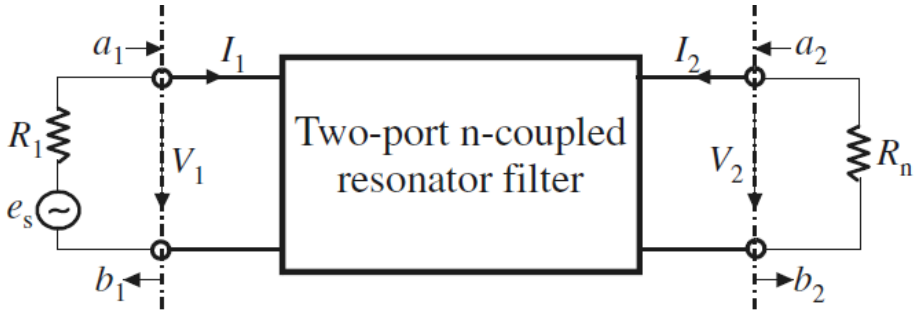

Figure 2.11: Network representation for the Equivalent circuit of magnetically n-coupled resonators in N-port network

$$a_1 = \frac{e_s}{2\sqrt{R_1}}, \qquad b_1 = \frac{e_s - 2i_1R_1}{2\sqrt{R_1}},$$
$$a_2 = 0, \qquad b_2 = i_n\sqrt{R_n}, \tag{2.27}$$

and hence,

$$S_{21} = \frac{b_2}{a_1}|a_2 = 0 = \frac{2\sqrt{R_1R_n}\, i_n}{e_s},$$
$$S_{11} = \frac{b_1}{a_1}\Big|a_2 = 0 = 1 - \frac{2R_1i_1}{e_s}, \tag{2.28}$$

Solving (2.24) for i_1 and i_n , we obtained,

$$i_1 = \frac{e_s}{\omega_0 L.FBW}\overline{[Z]}_{11}^{-1},$$
$$i_n = \frac{e_s}{\omega_0 L.FBW}\overline{[Z]}_{n1}^{-1}, \tag{2.29}$$

where $\overline{[Z]}_{ij}^{-1}$ denotes the ith row and jth column element of $\overline{[Z]}^{-1}$. Substituting (2.29) into (2.28) yields,

$$S_{21} = \frac{2\sqrt{R_1R_n}}{\omega_0 L.FBW}\overline{[Z]}_{n1}^{-1},$$
$$\text{and} \qquad S_{11} = 1 - \frac{2R_1}{\omega_0 L.FBW}\overline{[Z]}_{11}^{-1}, \tag{2.30}$$

For the external quality factors $q_{ei} = \omega_0 L.FBW/R_i$, the S-parameters become,

$$S_{21} = 2\frac{1}{\sqrt{q_{e1}.q_{en}}}\overline{[Z]}_{n1}^{-1},$$
$$S_{11} = 1 - \frac{2}{q_{e1}}\overline{[Z]}_{11}^{-1}, \tag{2.31}$$

where q_{e1} and q_{en} are the normalized external quality factors at the first and last resonators, respectively. In case of asynchronously tuned coupled-resonator circuit, resonators may have different resonant frequencies, and extra entries m_{ii} are added to the diagonal entries in $\overline{[Z]}$ to account for asynchronous tuning as follows,

$$\overline{[Z]} = \begin{bmatrix} \frac{1}{q_{e1}} + p - jm_{11} & -jm_{12} & \cdots & -jm_{1n} \\ -jm_{21} & p & \cdots & -jm_{2n} \\ \vdots & \vdots & \vdots & \vdots \\ -jm_{n1} & -jm_{n2} & \cdots & \frac{1}{q_{en}} + p - jm_{nn} \end{bmatrix} \quad (2.32)$$

2.6.1.2 Circuits with electrically coupled resonators:

This section presents the derivation of coupling coefficients for electrically coupled resonators in an N-port circuit, where the electric coupling is represented by capacitors. The normalized admittance matrix $\overline{[Y]}$ will be derived here in an analogous way to the derivation of the $\overline{[Z]}$ matrix in the previous section. Figure 2.10 (a) shows the equivalent circuit of electrically coupled n-resonators in an N-port network, where v_i denotes the node voltage, i_s represents the source current and G represents the conductance. According to the current law which is the other one of Kirchhoff's two circuit laws and states that the algebraic sum of the currents leaving a node in a network is zero. Using this law, the node voltage equations are formulated as follows [3],

$$\begin{aligned} &\left(G_1 + jwC_1 + \frac{1}{jwL_1}\right) v_1 - jwC_{12}v_2 \ \ldots - jwC_{1n}v_n = i_s, \\ &-jwC_{12}v_1 + \left(jwC_2 + \frac{1}{jwL_2}\right) v_2 \ \ldots - jwC_{2n}v_n = 0, \\ &\vdots \\ &-jwC_{n1}v_1 - jwC_{n2}v_2 + \ldots + \left(G_n + jwC_n + \frac{1}{jwL_n}\right) v_n = 0, \end{aligned} \quad (2.33)$$

where $C_{ab} = C_{ba}$ denotes the mutual capacitance between resonators a and b. The matrix form representation of these equations is as follows,

$$\begin{bmatrix} G_1 + jwC_1 + \frac{1}{jwL_1} & -jwC_{12} & \cdots & -jwC_{1n} \\ -jwC_{12} & jwC_2 + \frac{1}{jwL_2} & \cdots & jwC_{2n} \\ \vdots & \vdots & \vdots & \vdots \\ -jwC_{n1} & wC_{n2} & \ldots & G_n + jwC_n + \frac{1}{jwL_n} \end{bmatrix} \begin{bmatrix} v_1 \\ v_2 \\ \vdots \\ v_n \end{bmatrix} = \begin{bmatrix} i_s \\ 0 \\ \vdots \\ 0 \end{bmatrix} \quad (2.34)$$

or equivalently $[Y].[v] = [i]$, where $[Y]$ is the admittance matrix.

Assuming all resonators are synchronized at the same resonant frequency $\omega_0 = 1/\sqrt{LC}$, where $L = L_1 = L_2 = \cdots L_n$ and $C = C_1 = C_2 = \cdots \mathrm{C_n}$, the admittance matrix $[Y]$ can be expressed by $[Y] = \omega_0 C.FBW.\overline{[Y]}$, where FBW is the fractional bandwidth, and $\overline{[Y]}$ is the normalized admittance matrix, given by [10],

$$\overline{[Y]} = \begin{bmatrix} \frac{G_1}{\omega_0 C(FBW)} + P & -\frac{jwC_{12}}{\omega_0 C}\frac{1}{FBW} & \cdots & -\frac{jwC_{1n}}{\omega_0 C}\frac{1}{FBW} \\ -\frac{jwC_{21}}{\omega_0 C}\frac{1}{FBW} & P & \cdots & -\frac{jwC_{2n}}{\omega_0 C}\frac{1}{FBW} \\ \vdots & \vdots & \vdots & \vdots \\ -\frac{jwC_{n1}}{\omega_0 C}\frac{1}{FBW} & -\frac{jwC_{n2}}{\omega_0 C}\frac{1}{FBW} & \cdots & \frac{G_n}{\omega_0 C(FBW)} + P \end{bmatrix} \quad (2.35)$$

where P is the complex lowpass frequency variable.

By defining the coupling coefficient as $M_{ij} = C_{ij}/C$, and the external quality factor for the resonator as $Q_{ei} = \omega_0 C/G_i$, and assuming $\omega/\omega_0 \approx 1$ for narrow band approximation, the normalized admittance matrix $\overline{[Y]}$ may be simplified to,

$$\overline{[Y]} = \begin{bmatrix} \frac{1}{q_{e1}} + p & -jm_{12} & \cdots & -jm_{1n} \\ -jm_{21} & p & \cdots & -jm_{2n} \\ \vdots & \vdots & \vdots & \vdots \\ -jm_{n1} & -jm_{n2} & \cdots & \frac{1}{q_{en}} + p \end{bmatrix} \quad (2.36)$$

where $q_{ei} = Q_{ei}.FBW$ is the scaled external quality factor, and $m_{ij} = M_{ij}.FBW$ is the normalized coupling coefficient.

The network representation for the circuit in Figure 2.12, considering only two-ports, is shown in Figure 2.10 (a), a_1, b_1, a_2, b_2 where are the wave variables, V_1, I_1, V_2, I_2 are the

voltage and current variables, it can be identified that $V_1 = v_1, V_2 = -v_n$ and $I_1 = i_s - v_1 G_1$ then we have,

$$a_1 = \frac{i_s}{2\sqrt{G_1}}\ , \qquad b_1 = \frac{2v_1 G_1 - i_s}{2\sqrt{G_1}}\ ,$$
$$a_2 = 0\ , \qquad b_2 = v_n\sqrt{G_n}\ . \tag{2.36}$$

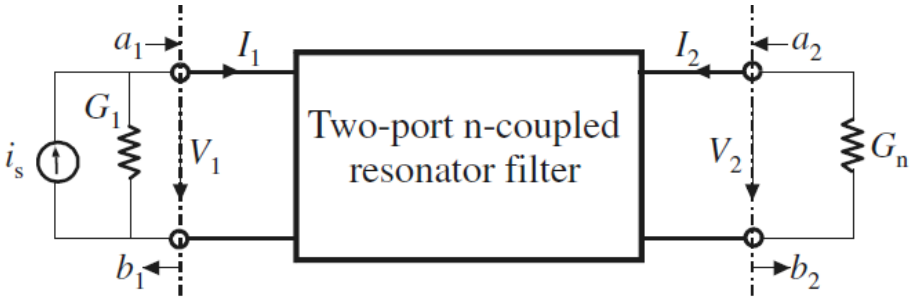

Figure 2.12: Network representation for the Equivalent circuit of electrically n-coupled resonators in N-port network.

$$S_{21} = \frac{b_2}{a_1}|a_2 = 0 = \frac{2\sqrt{G_1 G_n}\, v_n}{i_s}\ ,$$

$$S_{11} = \frac{b_1}{a_1}\Big|a_2 = 0 = \frac{2G_1 v_1}{i_s} - 1\ . \tag{2.37}$$

Solving (2.34) for v_1 and v_n , we obtained,

$$v_1 = \frac{i_s}{\omega_0 C.FBW}\overline{[Y]}_{11}^{-1}\ ,$$

$$v_n = \frac{i_s}{\omega_0 C.FBW}\overline{[Y]}_{n1}^{-1}\ , \tag{2.38}$$

where $\overline{[Y]}_{ij}^{-1}$ denotes the ith row and jth column element of $\overline{[Y]}^{-1}$. Substituting (2.38) into (2.37) yields,

$$S_{21} = \frac{2\sqrt{G_1 G_n}}{\omega_0 C.FBW}\overline{[Y]}_{n1}^{-1}$$

$$S_{11} = \frac{2G_1}{\omega_0 C.FBW}\overline{[Y]}_{11}^{-1} - 1 \tag{2.39}$$

For the external quality factors $q_{ei} = \omega_0 C.FBW/G_i$, the S-parameters become,

$$S_{21} = 2\frac{1}{\sqrt{q_{e1}.q_{en}}}\overline{[Y]}_{n1}^{-1}$$

$$S_{11} = \frac{2}{q_{e1}}\overline{[Y]}_{11}^{-1} - 1 \tag{2.40}$$

where q_{e1} and q_{en} are the normalized external quality factors at the resonator, In case of asynchronously tuned coupled-resonator circuit, resonators may have different resonant frequencies, and extra entries m_{ii} are added to the diagonal entries in $\overline{[Y]}$ to account for asynchronous tuning as follows,

$$\overline{[Y]} = \begin{bmatrix} \frac{1}{q_{e1}} + p - jm_{11} & -jm_{12} & \cdots & -jm_{1n} \\ -jm_{21} & p - jm_{22} & \cdots & -jm_{2n} \\ \vdots & \vdots & \vdots & \vdots \\ -jm_{n1} & -jm_{n2} & \cdots & \frac{1}{q_{en}} + p - jm_{nn} \end{bmatrix} \tag{2.41}$$

2.6.1.3 General coupling matrix:

From previous derivations in the last two sections, the most notable is that the formulation of normalized impedance matrix $\overline{[Z]}$ is identical to that of normalized admittance matrix $\overline{[Y]}$. Accordingly, a unified solution may be formulated regardless of whether the couplings are magnetic or electric or even the combination of both. So the S parameters of the n-coupled resonator filter may be generalized as [3],

$$S_{21} = 2\frac{1}{\sqrt{q_{e1}.q_{en}}}\overline{[A]}_{n1}^{-1}$$

$$S_{11} = \pm\left(1 - \frac{2}{q_{e1}}\overline{[A]}_{11}^{-1}\right) \tag{2.42}$$

with

$$[A] = [q] + p[U] - j[m] \tag{2.43}$$

where $[U]$ is the $n \times n$ unit or identity matrix, $[q]$ is an $n \times n$ matrix with all entries zeros, except for $q_{11} = 1/q_{e1}$ and $q_{nn} = 1/q_{en}$, $[m]$ is so-called general coupling matrix, which is an $n \times n$ reciprocal matrix $(m_{ij} = m_{ji})$ and is allowed to have nonzero diagonal entries

m_{ii} for an asynchronously tuned filter.

As this is clearly impractical, it is usually necessary to perform a sequence of similar transformations until a more convenient form for implementation is obtained. A more practical synthesis approach will be presented in the next chapter.

2.7 Optimization:

For design of filters, the computer-aided analysis techniques are used to evaluate filter performance. The sequence of filter analysis, comparison with the desired performance, and modification of designable parameters is performed iteratively until the optimum performance of the filter is achieved. This process is known as optimization [3].

Optimization techniques, generally share a common aim of minimization of a scalar cost function $U(\emptyset)$, where $\emptyset$ is a set of parameters known as control variables. At each iteration in the optimization process, some or all values of $\emptyset$ are modified, and the cost function is evaluated. This is repeated until an optimal solution is found such that the cost function is minimized [6]. The control variables may be either unconstrained, so that the search space is unbounded, or constrained by lower and upper limits to prevent the optimization algorithm from giving an unfeasible solution. In microwave coupled resonator optimization problems, the cost function of many variables depends on two methods, local optimization methods or global optimization methods.

Local optimization methods depend on the initial values of the control parameters. The initial estimation should be given as an input to the algorithm that will search on a local minimum within the local neighborhood of the initial estimation.

Global optimization algorithms generally do not require initial estimation for the control variables, and generate their own initial values, and they search on the global minimum within the entire search space.

In comparison to local methods, global optimization methods are much slower and may take hours or even days to find the optimal solution for problems with tens of variables. Global algorithms tend to be utilized when the local algorithms are not adequate, or when it is of great importance to find the global solution [6].

There is a large number of optimization methods, for global optimization method, we used Genetic algorithm [3], but for local optimization method we used both Nelder Mead Simplex algorithm and Interpolated Quasi Newton [7]. All these optimization techniques

are available in simulation software CST that has been utilized in the design as will be shown later in next chapters.

2.7.1 Cost Function:

The problem of optimization may be formulated as minimization of the cost function $U(\emptyset)$, because it represents the difference between the performance achieved at any stage and the desired specifications. In the case of a microwave filter and multiplexer, the formulation of $U(\emptyset)$ may involve the specified and achieved values of the insertion loss and the return loss in the passband, and the rejection in the stopband. $\emptyset$ is the set of designable parameters whose values may be modified during the optimization process. Elements of $\emptyset$ could be the values of capacitors and inductors for a lumped-element or coupling coefficients for a coupled resonator circuit [3].

Usually, there are various constraints on the designable parameters for a feasible solution obtained by optimization. For example, available or achievable values of lumped elements, the minimum values of microstrip line width, and coupled microstrip line spacing that can be etched. The elements of $\emptyset$ define a space. A portion of this space where all the constraints are satisfied is called the design space D. In the optimization process, we look for optimum value of $\emptyset$ inside D. A global minimum of $U(\emptyset)$, located by a set of design parameters $\emptyset_{min}$, is such that [3]:

$$U_{min} = U(\emptyset_{min}) < U(\emptyset) \ , \tag{2.44}$$

for any feasible $\emptyset$ not equal to $\emptyset_{min}$. However, an optimization process does not generally guarantee finding a global minimum but yields a local minimum, which may be defined as follows:

$$U(\emptyset_{min}) = \text{minimize}_{\emptyset \in D_L} U(\emptyset) \, , \tag{2.45}$$

where D_L is a part of D in the local vicinity of $\emptyset_{min}$. If this situation happens, one may consider starting the optimization again with another set of initial designable parameters, or to change another optimization method that could be more powerful to search for the global minimum, or even to modify the objective function.

Summary:

In this chapter, the theory of filter design is studied. The design starts from a lowpass prototype circuit that is then transformed to bandpass circuit. Theory of coupling has been presented as well as optimization techniques that are used in the filter deign.

References

[1] M. Alaydrus, "Designing Microstrip Bandpass Filter at 3.2 GHz," International Journal on Electrical Engineering and Informatics – Vol.2, No.2, 2010.

[2] V. Jadaun, P. Sharma, H. Gupta and D. Mahor, "Design a Microstrip Band Pass Filter for 6 GHz," International Journal of Engineering and Technology, Vol.1, No.3, pp.217-222, 2012.

[3] J. Hong and M. J. Lancaster, Microstrip Filters for RF/Microwave Applica- tions, John Wiley & Sons, Inc.,NY, 2001.

[4] P. Terblanche, "Electronically Adjustable Bandpass Filter," MSc dissertation, Univ. of Stellenbosch, Electrical and Electronic Engineering Dept., South Africa, 2011.

[5] T. Skaik, "Multilayer Microwave Filter with stacked spirals," MSc dissertation, Univ. of Birmingham, Electrical and Electronics Engineering Dept., UK, 2007.

[6] T. Skaik, "A Synthesis of Coupled Resonator Circuits with Multiple Outputs using Coupling Matrix Optimization", PhD Thesis, March 2011, School of Electronic, Electrical and Computer Engineering, the University of Birmingham.

[7] A. Ravindran, K. M. Ragsdell and G. V. Reklaitis. Engineering Optimization Methods and Applications, John Wiley & Sons, Inc., Hoboken, New Jersey, 2006.

Chapter 3

Microstrip Lines and Hairpin Resonators

3.1 Microstrip Transmission Line:

Microstrip transmission line is the most used planar transmission line in radio frequency (RF) applications. The planar configuration can be achieved by several ways, for example with the photolithography process or thin-film and thick film technology. As other transmission line in RF applications, microstrip can also be exploited for designing certain components, like filter, coupler, transformer or power divider [1].

The microstrip structure consists of a conducting strip with thickness t and width W located on top of a dielectric material (substrate) with dielectric constant ε_r and height h as shown in figure 3.1. The bottom of structure is a ground (conducting) plane [2].

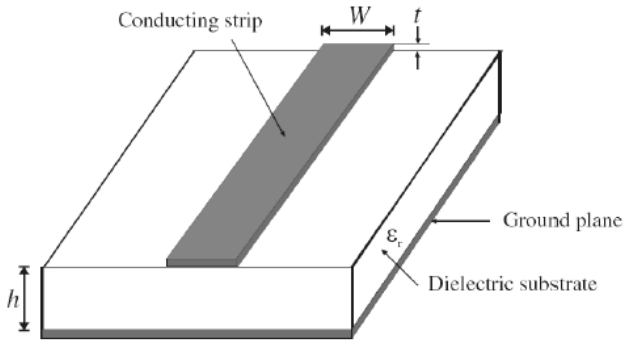

Figure 3.1: Microstrip structure

3.1.1 Waves in Microstrips:

The fields in the microstrip extend within two media, air above and dielectric below so that the structure is inhomogeneous. Hence microstrip transmission lines do not support pure TEM waves [2]; figure 3.2 shows the behavior of electric and magnetic field lines [3].

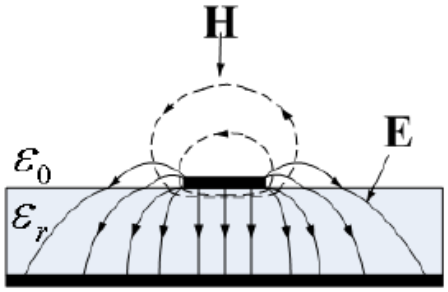

Figure 3.2: Electric and magnetic field lines.

3.1.2 Effective Dielectric Constant and Characteristic Impedance:

Transmission characteristics of microstrips are described by two parameters, namely, the effective dielectric constant ε_{re} and characteristic impedance Z_c, and they are determined from the values of two capacitances as follows [2]:

$$\varepsilon_{re} = \frac{C_d}{C_a}, \tag{3.1}$$

$$Z_c = \frac{1}{c\sqrt{C_a C_d}}, \tag{3.2}$$

where:

C_d: The capacitance per unit length with the dielectric substrate present.

C_a: The capacitance per unit length with the dielectric substrate replaced by air.

c: The velocity of electromagnetic waves in free space ($c \approx 3.0 \times 10^8$ m/s).

For very thin conductors (t ≈ 0), equations for dielectric constant and characteristic impedance that provides accuracy better than 1% are as follows [2]:

For $W/h \leq 1$:

$$\varepsilon_{re} = \frac{\varepsilon_{re}+1}{2} + \frac{\varepsilon_{re}-1}{2}\left\{\left(1 + 12\frac{h}{W}\right)^{-0.5} + 0.04\left(1 - \frac{W}{h}\right)^2\right\}, \tag{3.3}$$

$$Z_c = \frac{\eta}{2\pi\sqrt{\varepsilon_{re}}}\ln\left(\frac{8h}{W} + 0.25\frac{W}{h}\right), \tag{3.4}$$

where $\eta = 120\pi$ ohms is the wave impedance in free space.

For $W/h \geq 1$:

$$\varepsilon_{re} = \frac{\varepsilon_{re}+1}{2} + \frac{\varepsilon_{re}-1}{2}\left(1 + 12\frac{h}{W}\right)^{-0.5}, \tag{3.5}$$

$$Z_c = \frac{\eta}{\sqrt{\varepsilon_{re}}}\left\{\frac{W}{h} + 1.393 + 0.677\ln\left(\frac{W}{h} + 1.444\right)\right\}^{-1}, \tag{3.6}$$

3.1.3 Guided Wavelength and Propagation Constant:

The guided wavelength in mm of the quasi-TEM mode of microstrip is given by [2]:

$$\lambda_g = \frac{300}{f(GHz)\sqrt{\varepsilon_{re}}} mm \tag{3.7}$$

where f is the operation frequency in GHz.

The propagation constant β can be determined by [2]:

$$\beta = \frac{2\pi}{\lambda_g} \tag{3.8}$$

3.1.4 Phase velocity and Electrical Length:

The phase velocity v_p can be determined by [2]:

$$v_p = \frac{w}{\beta} = \frac{c}{\sqrt{\varepsilon_{re}}} , \tag{3.9}$$

The electrical length θ for a given physical length l of the microstrip is defined by [2]:

$$\theta = \beta l , \tag{3.10}$$

Therefore, $\theta = \pi/2$ when $l = \lambda_g/4$, and $\theta = \pi$ when $l = \lambda_g/2$, these quarter wavelength and half-wavelength microstrip lines are important for design of microstrip filters.

3.1.5 Synthesis of W/h:

For a given characteristic impedance Z_c and effective dielectric constant ε_{re} and substrate thickness h, the equations used to calculate the strip width (W) are as follows [2]:

For $W/h \leq 2$:

$$\frac{W}{h} = \frac{8\exp(A)}{\exp(2A)-2} , \tag{3.11}$$

with

$$A = \frac{Z_c}{60}\left\{\frac{\varepsilon_r+1}{2}\right\}^{0.5} + \frac{\varepsilon_r-1}{\varepsilon_r+1}\left\{0.23 + \frac{0.11}{\varepsilon_r}\right\} , \tag{3.12}$$

For $W/h \geq 2$:

$$\frac{W}{h} = \frac{2}{\pi}\left\{(B-1) - \ln(2B-1) + \frac{\varepsilon_r-1}{2\varepsilon_r}\left[\ln(B-1) + 0.39 - \frac{0.61}{\varepsilon_r}\right]\right\} , \tag{3.13}$$

with,

$$B = \frac{60\pi^2}{Z_c\sqrt{\varepsilon_r}} \ . \tag{3.14}$$

3.2 Resonators:

A resonator is a device that stores energy, but in two different ways. The system resonates by exchanging the energy stored from one way to another. In a LC resonator the energy is exchanged between the inductor, where it is stored as magnetic energy, and the capacitor, where it is stored as electric energy. Resonance occurs at the frequency where the average stored magnetic and electric energies are equal [4].

There are numerous forms of microstrip resonators. In general, microstrip resonators for filter designs may be classified as lumped-element or quasi lumped-element resonators and distributed line or patch resonators. Some typical configurations of these resonators are illustrated in figure 3.3 [2]. In this project the resonator used is the hairpin (U-shaped) resonator as explained in the next section.

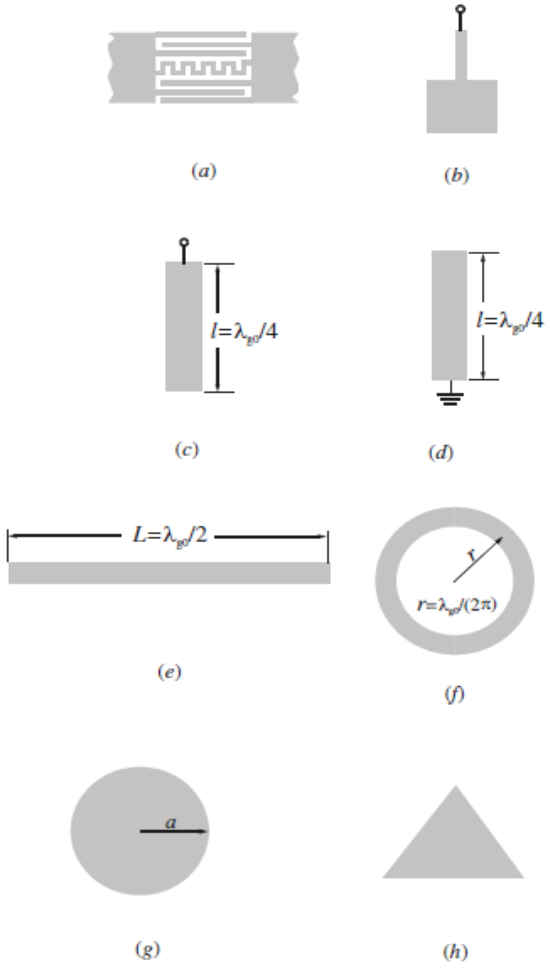

Figure 3.3: Some typical microstrip resonators: (*a*) lumped-element resonator; (*b*) quasilumped element resonator; (*c*) $\lambda_{g_0}/4$ line resonator (shunt series resonance); (*d*) $\lambda_{g_0}/4$ line resonator (shunt parallel resonance); (*e*) $\lambda_{g_0}/2$ line resonator; (*f*) ring resonator; (*g*) circular patch resonator; (*h*) triangular patch resonator.

3.2.1 Hairpin Resonator:

The hairpin resonator filter is one of the most popular microstrip filter configurations used in the lower microwave frequencies. It is easy to manufacture because it has open-circuited ends that require no grounding. Its form is derived from the edge-coupled resonator filter by folding back the ends of the resonators into a "U" shape; this reduces the length and improves the aspect ratio of the microstrip [6]. Moreover, this resonator structure has the advantage of compact size and low cost.

Figure 3.4(a) shows a conventional hairpin resonator that may be miniaturized by loading a lumped-element capacitor between the both ends of the resonator, as indicated in figure 3.4(b), or alternatively with a pair of coupled lines folded inside the resonator as shown in figure 3.4(c) [2].

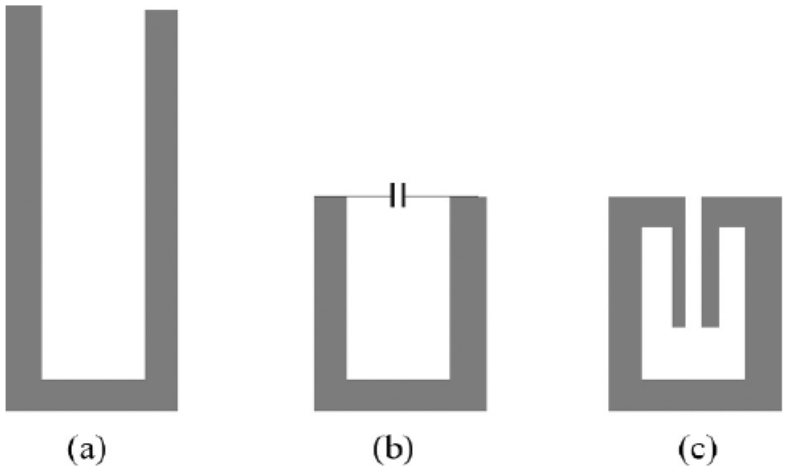

Figure 3.4: Structural variations to miniaturize hairpin resonator. (a) Conventional hairpin resonator. (b) Miniaturized hairpin resonator with loaded lumped capacitor. (c) Miniaturized hairpin resonator with folded coupled lines.

Tapped line input and coupled line input are the two types of hairpin structures that are commonly used in filter realization and are shown in figure 3.5 (a) and (b) respectively. Tapped line input has a space saving advantage over coupled line input, while designing the coupling line is required for the input and output high external quality factor [2].

In this thesis, the filter is designed to have input and output tapped lines. The tapped lines are chosen to have characteristic impedances of 50 Ω.

3.2.2 Hairpin Coupling Structures:

The three basic coupling structures are shown in figure 3.6. The coupled structures result from different orientations of a pair of identical hairpin resonators. It is clear that any

coupling in those coupling structures is that of the proximity coupling, which is, basically, through fringe fields [9]. The nature and the extent of the fringe fields determine the nature and the strength of the coupling. It can be shown that at resonance, each of the hairpin resonators has the maximum electric field intensity at the side with an open side, and the maximum magnetic field intensity at the opposite side.

Because the fringe field exhibits an exponentially decaying character outside the region, the electric fringe field is stronger near the side having the maximum electric field distribution, while the magnetic fringe field is stronger near the side having the maximum magnetic field distribution [9].

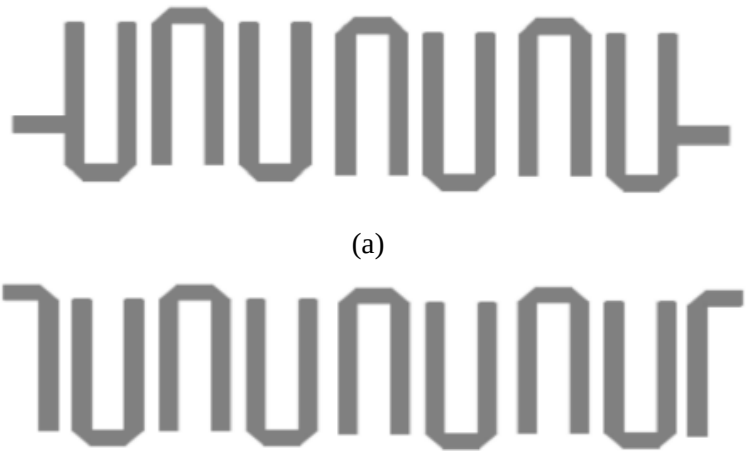

(a)

(b)

Figure 3.5: Hairpin Structures. (a) Tapped line input Hairpin filter. (b) Coupled line input Hairpin filter.

The electric coupling can be obtained if the open sides of two coupled resonators are proximately placed as figure 3.6 (a) shows, while the magnetic coupling can be obtained if the sides with the maximum magnetic field of two coupled resonators are proximately placed as figure 3.6 (b) shows. For the coupling structure in figure 3.6 (c), the electric and magnetic fringe fields at the coupled sides may have comparative distributions so that both the electric and the magnetic couplings occur [2]. In this case the coupling may be referred to as the mixed coupling.

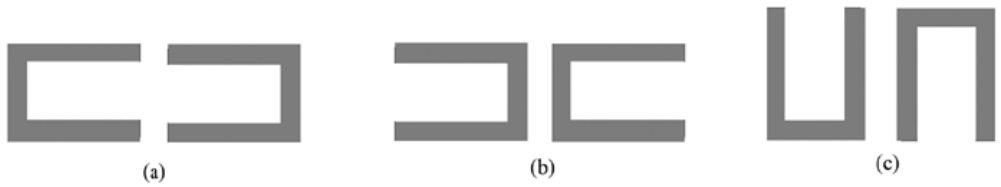

Figure 3.6: Basic coupling structures of coupled microstrip hairpin resonators. (a) Electric coupling structure. (b) Magnetic coupling structure. (c) Mixed coupling structure.

3.2.3 Unloaded quality factor:

The unloaded quality factor Q_u is a figure of merit for a resonator. It describes the quality of the resonator in terms of losses and energy storage. For example, a high Q resonator implies low energy loss and good energy storage, whereas a low Q implies higher losses. A general definition for the Q_u that applies to any type of resonator is [2],

$$Q_u = \omega \frac{\text{Time – average energy stored in the resonator}}{\text{Average power lost in the resonator}} \tag{3.15}$$

The losses in a resonator can generally be associated with the conductor, dielectric material, and radiation. The total Q_u may be defined by adding these losses together as follows [2],

$$\frac{1}{Q_u} = \frac{1}{Q_c} + \frac{1}{Q_d} + \frac{1}{Q_r} \ , \tag{3.16}$$

where Q_c , Q_d and Q_r are the quality factors associated with losses from conductor and dielectric making up the resonator and radiation from the cavity. The loaded quality factor Q_L may be defined in terms of the unloaded quality factor Q_u and the external quality factor Q_e as follows [10],

$$\frac{1}{Q_L} = \frac{1}{Q_u} + \frac{1}{Q_e} , \tag{3.17}$$

where Q_e is the quality factor associated with effective losses through the external coupling circuit, and it is defined as the ratio of the energy stored in the resonator to the energy coupled to the external circuit. The extraction of the external quality factor from the physical structure will be described in the next section. The conductor quality factor is adversely proportional to the surface resistance of the conductor sheets. At low frequencies, the total dc resistance of hairpin is defined as [7]:

$$R_{dc} = \frac{l}{Wt\sigma} \ , \tag{3.18}$$

where l the total length of the conductor, W is the track width of the hairpin, t is the thickness, and σ is the conductivity of the conductor. At high frequencies, the resistance is defined as [7]:

$$R_{rf} = \frac{l}{W\sigma\delta\left(1-e^{\frac{1}{\delta}}\right)}\ , \tag{3.19}$$

where δ is the skin depth and is defined by [8]:

$$\delta = \sqrt{\frac{2}{\omega\mu\sigma}} \tag{3.20}$$

The dielectric quality factor Q_d is adversely proportional to the loss tangent of the dielectric substrate. For a substrate with very high resistivity, the loss tangent is very small, and the ohmic losses in the dielectric material are very small, whereas for a substrate with very low resistivity, the electric field penetration inside the substrate is limited and the ohmic losses take place in this case [7].

The radiation quality factor Q_r is generally defined as [2]:

$$Q_r = \omega \frac{\text{Time – average energy stored in the resonator}}{\text{Average power radiated}} \tag{3.21}$$

Normally, the filters are shielded in housing walls, so the power radiated will be lost in the imperfect conducting walls [2].

3.2.4 Extracting internal coupling coefficients:

Coupling between resonators may be electric, magnetic and mixed coupling. At the same resonant frequency, the coupled resonators are synchronously tuned, while when they are different, the coupled resonators are asynchronously tuned. The general formula to extract any coupling coefficient for tuned coupled resonators is as follows [2]:

$$k = \pm\frac{1}{2}\left(\frac{f_{02}}{f_{01}} + \frac{f_{01}}{f_{02}}\right)\sqrt{\left(\frac{f_{p2}^2 - f_{p1}^2}{f_{p2}^2 + f_{p1}^2}\right)^2 - \left(\frac{f_{02}^2 - f_{01}^2}{f_{02}^2 + f_{01}^2}\right)^2}\ , \tag{3.22}$$

where $f_{0i} = \omega_{0i}/2\pi$ and $f_{pi} = \omega_i/2\pi$ $i = 1,2$.

For synchronous tuned coupled resonators, $f_{01} = f_{02}$ then [2]:

$$k = \pm \frac{f_{p2}^2 - f_{p1}^2}{f_{p2}^2 + f_{p1}^2} \ , \qquad (3.23)$$

where f_{p1} is the lower frequency of the band and f_{p2} is the upper frequency.

The coupling coefficient sign depends on the coupling structure of the coupled resonators.

When using CST microwave studio EM simulator, the coupling between any pair of resonators is controlled by the spacing between the resonators. The coupled pair of the resonators is excited by weak coupling from ports as in figure 3.7.

Then, the two resonant peaks resulting from coupling between the two resonators can be observed from the EM-simulated frequency responses as shown in figure 3.8. The coupling coefficient can then be calculated using equation (3.22).

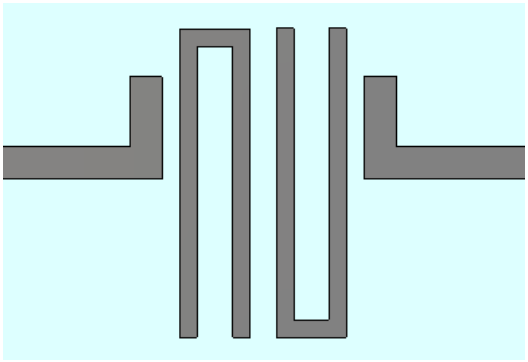

Figure 3.7: Two coupled hairpin resonators.

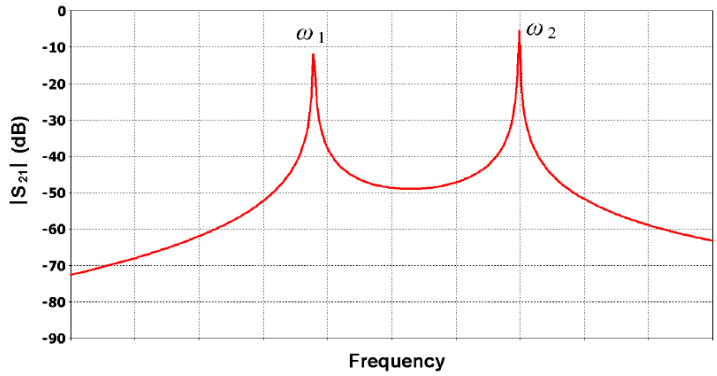

Figure 3.8: Amplitude response of S_{21} for two coupled resonators.

3.2.5 Extracting external quality factor:

From the input/output (I/O) coupling structures for coupled microstrip resonator filters, namely the tapped line as shown in figure 3.9, the external quality factor is computed by [2]:

$$Q_e = \frac{f_0}{\Delta f_{3dB}} \ , \qquad (3.24)$$

where:

f_0: is the resonant frequency.

Δf_{3dB}: is the 3-dB bandwidth for S_{21} as in figure 3.10.

Using CST Microwave studio, the resonator is excited at port 1 through a 50 Ω coupled line, and port 2 is coupled weakly to the resonator. The 3-dB bandwidth of the magnitude response of S_{21} is then found for extracting the external quality factor Q_e .The external quality factor Q_e can then be calculated from the simulated S_{21} response using equation (3.24).

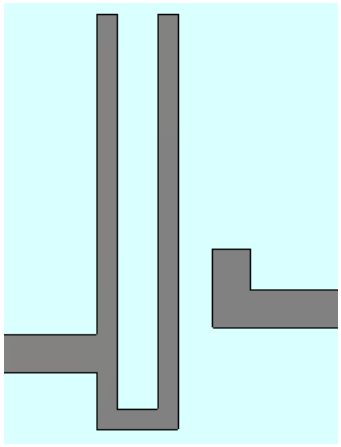

Figure 3.9: Tapped line external coupling

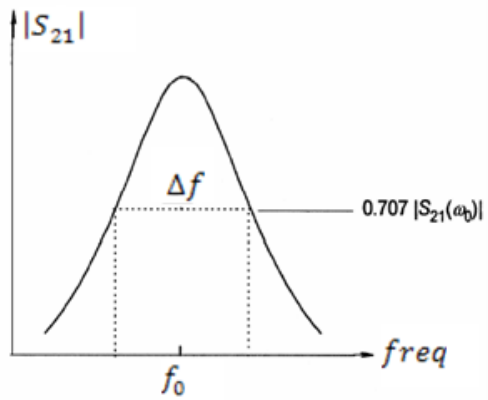

Figure 3.10: Amplitude response of S_{21} for externally coupled resonator.

After this work, we will go to the next chapter to the design and simulation of the microstrip hairpin filters that will be used to design our DCS/ UMTS/ LTE triplexer and UMTS/ LTE diplexer.

3.3 Summary:

In this chapter, the design equations of microstrip transmission line are presented. There are different types of resonators presented, and we explained why we used the hairpin resonator in the thesis. The difference between electric, magnetic and mixed coupling and how to use each of them is explained. Extracting internal and external coupling coefficients between resonators theoretically and practically using CST microwave studio is explained.

References:

[1] M. Alaydrus, "Designing Microstrip Bandpass Filter at 3.2 GHz," International Journal on Electrical Engineering and Informatics – Vol.2, No.2, 2010.

[2] J. Hong and M. J. Lancaster, Microstrip Filters for RF/Microwave Applications, John Wiley & Sons, Inc., NY, 2001.

[3] D. Zayniyev, " Development of planar filters and diplexers for wireless transceiver front ends," PhD thesis, 2010, School of Electronics and Computer Science, University of Westminster.

[4] P. Terblanche, "Electronically Adjustable Bandpass Filter" MSc dissertation, Univ. of Stellenbosch, Electrical and Electronic Engineering Dept., South Africa, 2011.

[5] K.Vidhya and T.Jayanthy, "Design of Microstrip Hairpin Band Pass Filter using Defected Ground Structure and Open Stubs," International Conference on Information and Electronics Engineering, IPCSIT vol.6, 2011.

[6] C. Salamat, M. Lorenzo and E. Roxas Jr, "Design of a narrowband hairpin filter on PTFE laminate," Communications Engineering Division, Advanced Science and Technology Institute**,** Quezon City Philippines 1101**.**

[7] I. Bahl, Lumped Elements for RF and Microwave Circuits, Artech House, Inc., Boston, 2003.

[8] CST Website, [Online]. Available: http://www.cst.com/content/products/mws/FIT.aspx

[9] J. Hong and M. Lancaster, "Coupling of Microstrip Square Open-Loop Resonators for Cross-Coupled Planar Microwave Filters," IEEE Transactions on Microwave Theory and Techniques, vol. 44, no.12, December 1996, pp. 2099-2109.

[10] D. Pozar, Microwave Engineering. 2nd edition, Wiley, 1998.

Chapter 4

Filter Simulation and Analysis

In this chapter, we will present the design of hairpin filters for DCS, UMTS and LTE systems. The coupling coefficients and the external quality factors will be computed for each filter.

4.1 DCS Filter:

A bandpass microstrip 5-pole filter with a fractional bandwidth 9.48% at a center frequency 1.793 GHz is designed for DCS system. RT/ Duroide 6006 substrate with height 1.27 mm, effective dielectric constant $\varepsilon_{re} = 6.15$, is chosen for the design. The input/output impedance of the feeding lines is 50 Ω and the resonator characteristic impedance is 68.3 Ω.

For n = 5, from table 2.1, the g-values are as follows:

$g_0 = g_6 = 1$
$g_1 = g_5 = 1.1468$
$g_3 = 1.975$
$g_2 = g_4 = 1.3712$

The equality between $g_0 = g_6$, $g_1 = g_5$, $g_2 = g_4$ is because of symmetry.

Wave length $(\lambda) = \frac{c}{f\sqrt{\varepsilon_{re}}} = \frac{300}{1.793\times10^9\times\sqrt{6.15}} = 67.4694\ mm$, $\frac{\lambda}{2} = 33.7347$

External coupling: $Q_{e1} = Q_{e5} = \frac{g_0 g_1}{FBW} = \frac{g_5 g_6}{FBW} = 12.0953$

$$k_0 = k_5 = \frac{1}{Q_{e1}} = \frac{1}{Q_{e5}} = 0.0827$$

Internal coupling: $k_1 = k_4 = \frac{FBW}{\sqrt{g_1 g_2}} = 0.0756$

$$k_2 = k_3 = \frac{FBW}{\sqrt{g_2 g_3}} = 0.0576$$

The calculated external quality factors and the coupling coefficients are achieved by utilizing CST simulation software as follows:

- External quality factor:
  From figure 4.1, the external coupling coefficient is,

$$Q_e = \frac{f_0}{\Delta f_{3dB}} = \frac{1.793}{0.10315} = 11.9358$$

$$k_0 = k_5 = \frac{1}{Q_e} = \frac{1}{3.6822} = 0.0838$$

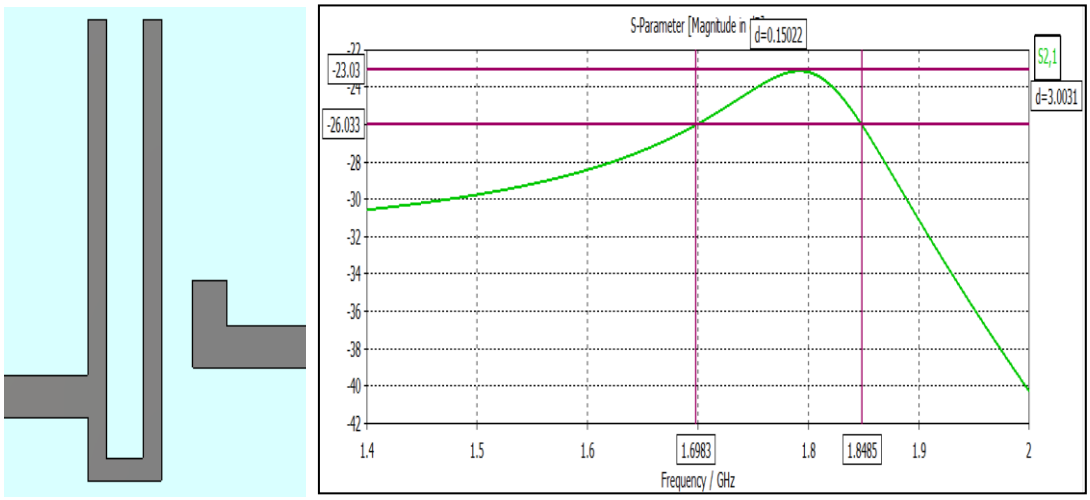

(a) (b)

Figure 4.1: DCS External coupling: (a) resonator design (b) S_{21} response

- Internal coupling coefficients:

  1- From figure 4.2, the coefficients between resonator 1,2 and 4,5 are as follows:

$$k_{1,2} = k_{4,5} = \frac{f_2^2 - f_1^2}{f_2^2 + f_1^2} = 0.0753$$

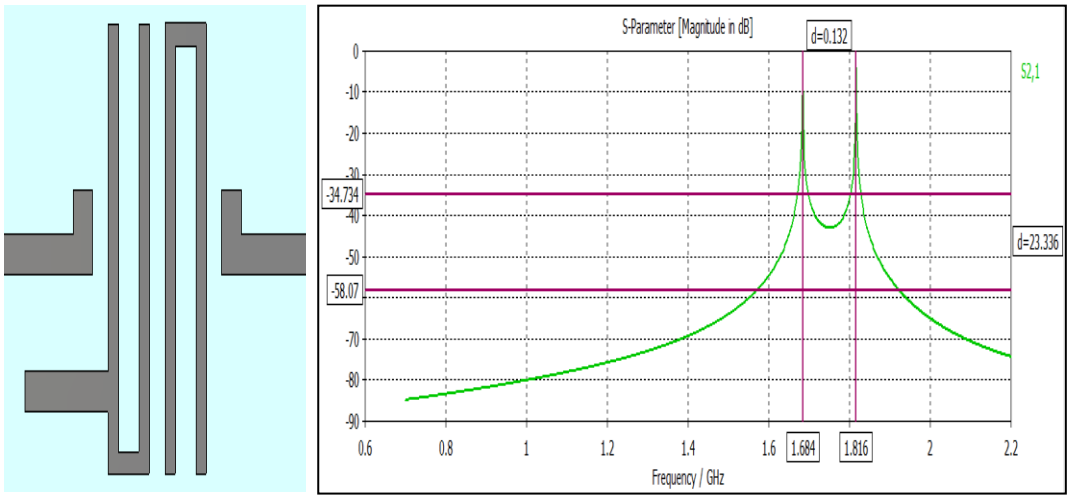

(a) (b)

Figure 4.2: DCS Internal coupling coefficients: (a) Resonator 1, 2 and 4, 5 design (b) S_{21} response

2- From figure 4.3, the coefficients between resonator 2,3 and 3,4 are as follows:

$$k_{2,3} = k_{3,4} = \frac{f_2^2 - f_1^2}{f_2^2 + f_1^2} = 0.0575$$

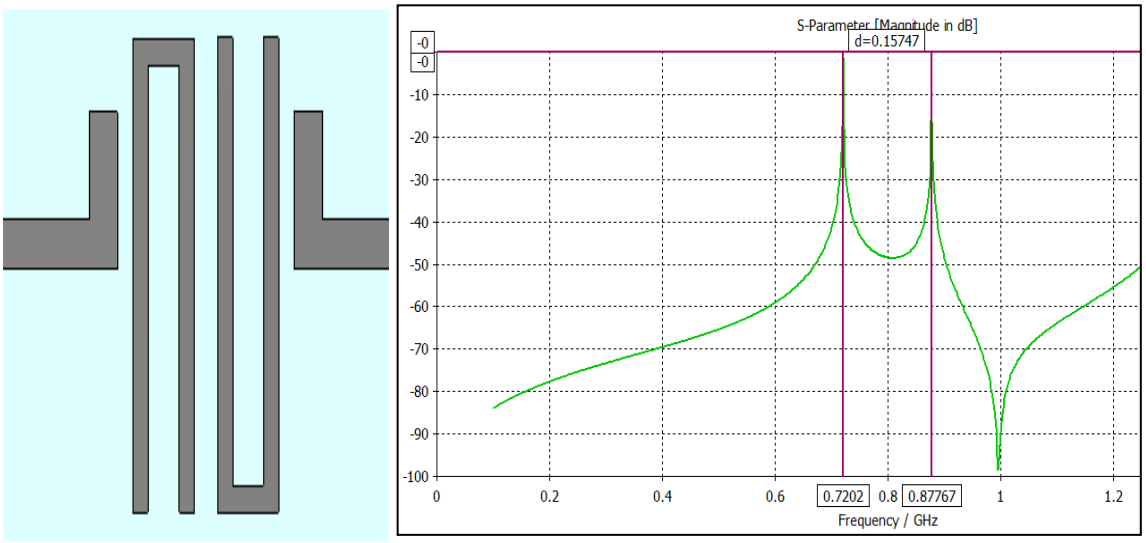

(a) (b)

Figure 4.3: DCS Internal coupling coefficients: (a) Resonator 2, 3 and 3, 4 design (b) S_{21} responses

- The structure of the 5-pole hairpin DCS filter is shown in figure 4.4 and the initial response is depicted in figure 4.5:

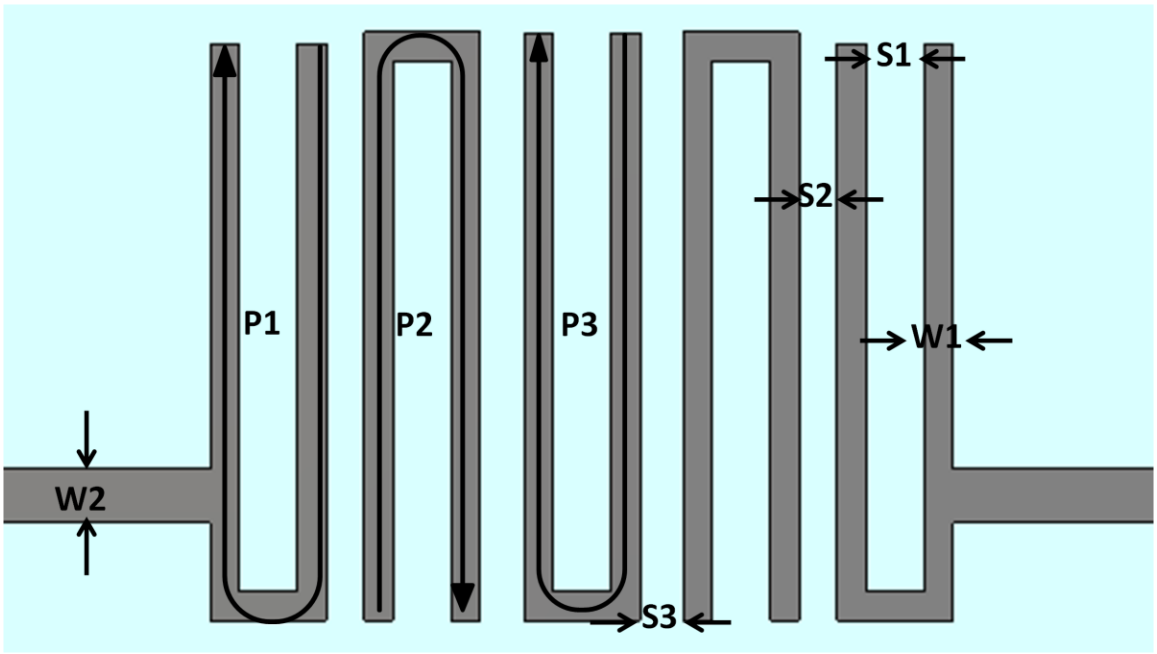

Figure 4.4: DCS 5-pole hairpin filter layout.

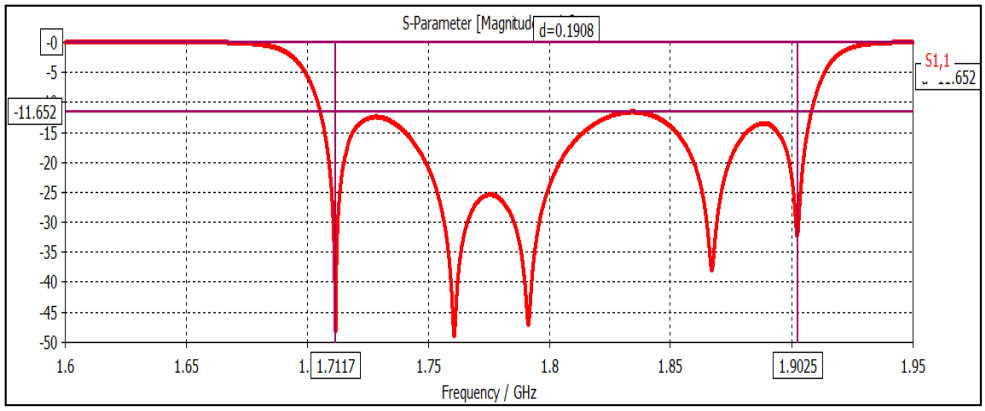

(a)

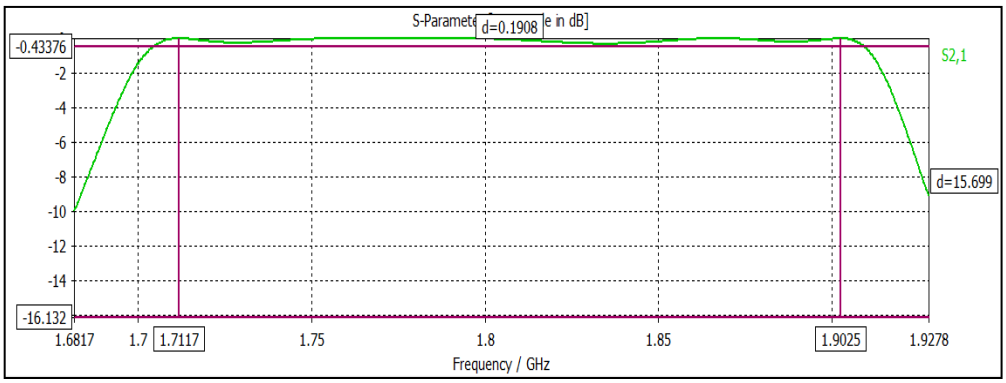

(b)

Figure 4.5: DCS 5-pole hairpin filter initial response (a) S_{11} response (b) S_{21} response

- After some modifications on the parameters of the filter, using both parameter sweep and optimization techniques in CST, the final response is shown in figure 4.6. The obtained return loss is about -15 dB and the passband ripple is about -0.13 dB.

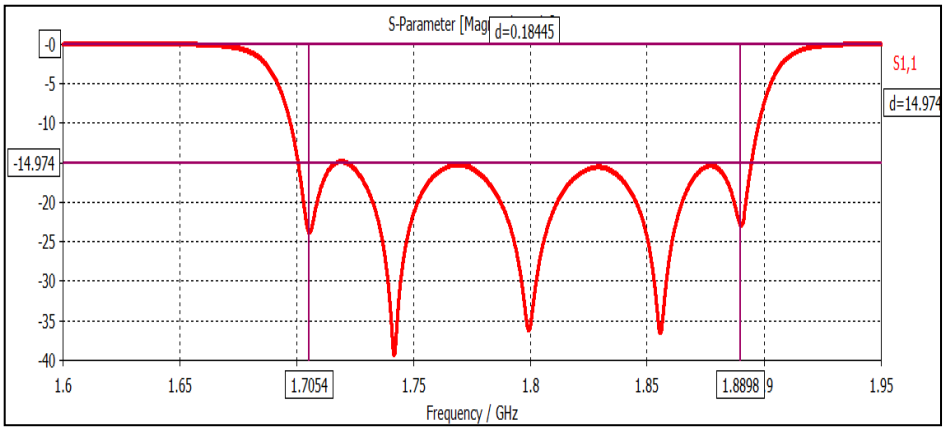

(a)

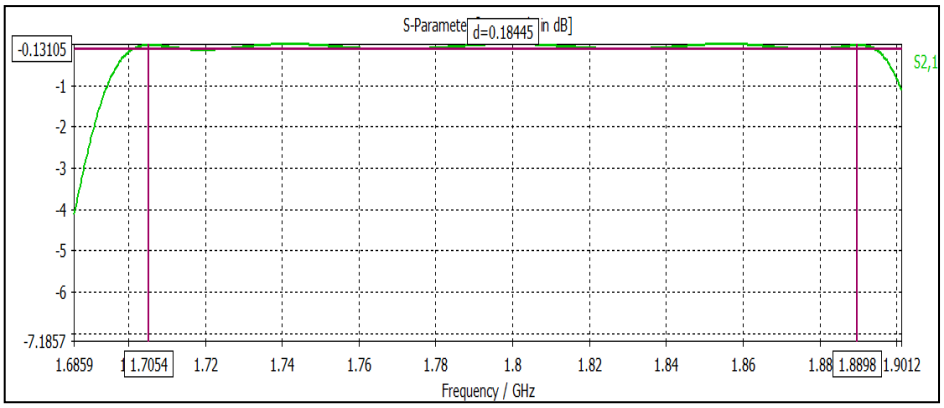

(b)

Figure 4.6: DCS 5-pole hairpin filter final response (a) S_{11} response (b) S_{21} response.

- A comparison between the initial and final parameters is shown in table 4.1.

Table 4.1: DCS initial and final parameters.

Parameter	Initial value (mm)	Final value (mm)
Spacing between the arms of the resonator (S1)	2	2
Spacing between resonator 1,2 & 4,5 (S2)	1.267	1.277
Spacing between resonator 2,3 & 3,4 (S3)	1.487	1.497
Length of the 1st and 5th resonators (P1)	41.5179	41.7179
Length of the 2nd and 4th resonators (P2)	42.3306	42.5306
Length of the 3rd resonator (P3)	42.1982	42.3982
Width of the 1st ,2nd ,3rd, 4th and 5th resonators (W1)	1	1
Width of the feed input/output (W2)	1.85	1.85

4.2 UMTS Filter:

A bandpass microstrip 5-pole filter with a fractional bandwidth 12.25% at a center frequency 2.0412 GHz is designed for UMTS system. RT/ Duroide 6006 substrate with height 1.27 mm, effective dielectric constant of $\varepsilon_{re} = 6.15$, is selected for the design. The input/output characteristic impedance of feeding lines is 50 Ω and resonator impedance is 68.3 Ω.

Figure 4.7 shows the design of the filter, and figure 4.8 gives us the initial response.

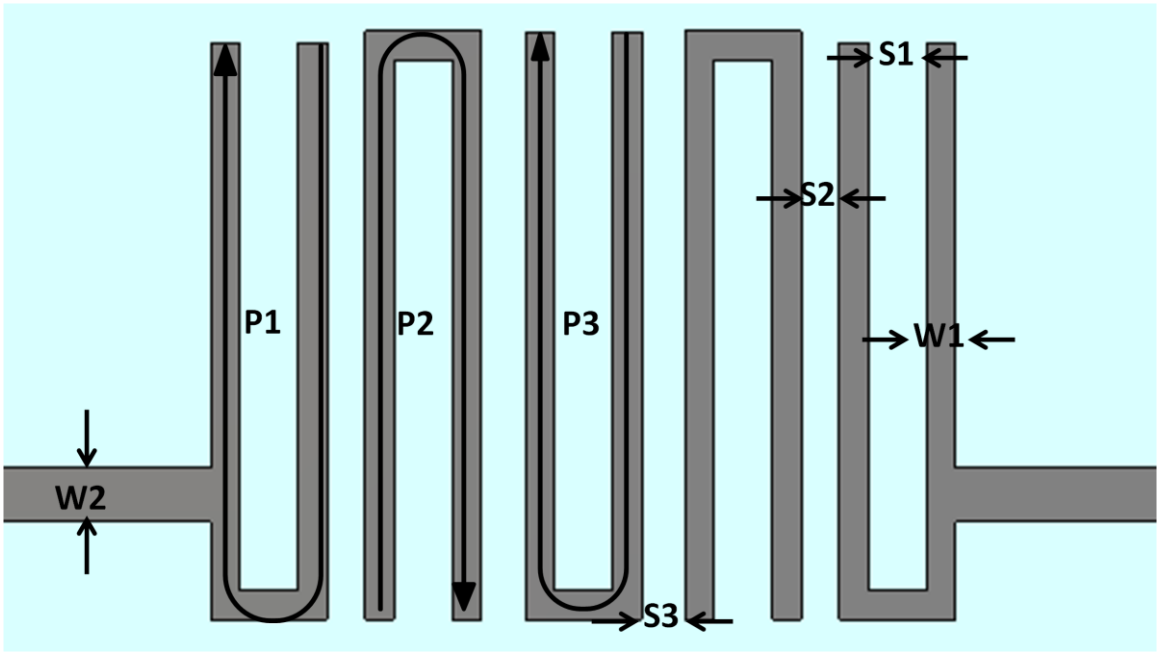

Figure 4.7: UMTS 5-pole hairpin filter layout.

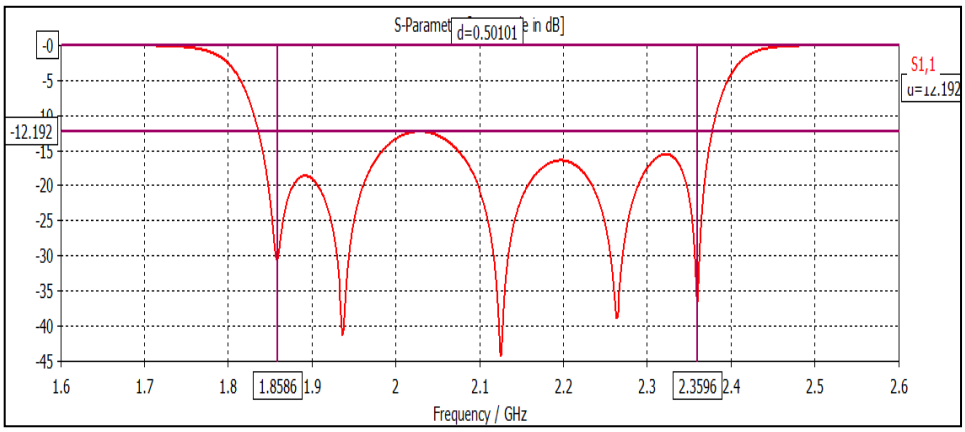

(a)

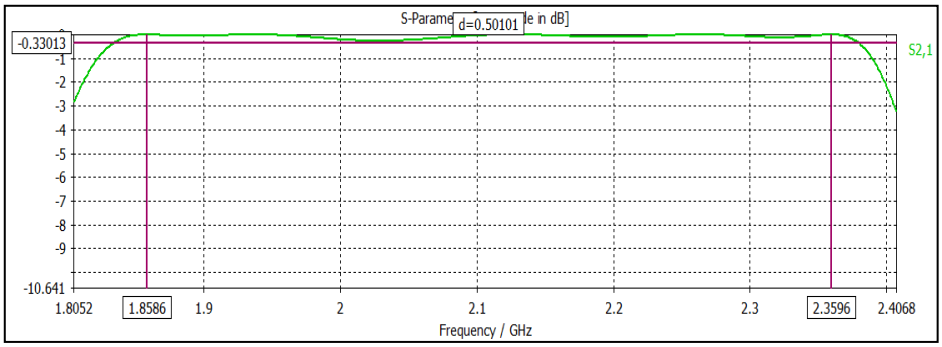

(b)

Figure 4.8: UMTS 5-pole hairpin filter initial response (a) S_{11} response (b) S_{21} response.

As in figure 4.8, the return loss of the initial response is about -12.1 dB and the passband ripple is about -0.33 dB. This result needs more modifications on the coupling coefficients, resonator lengths and the external couplings. The final results are presented in figure 4.9 which gives us a return of about -15.5 dB and a ripple passband about -0.1 dB, and table 4.2 shows the initial and final parameters.

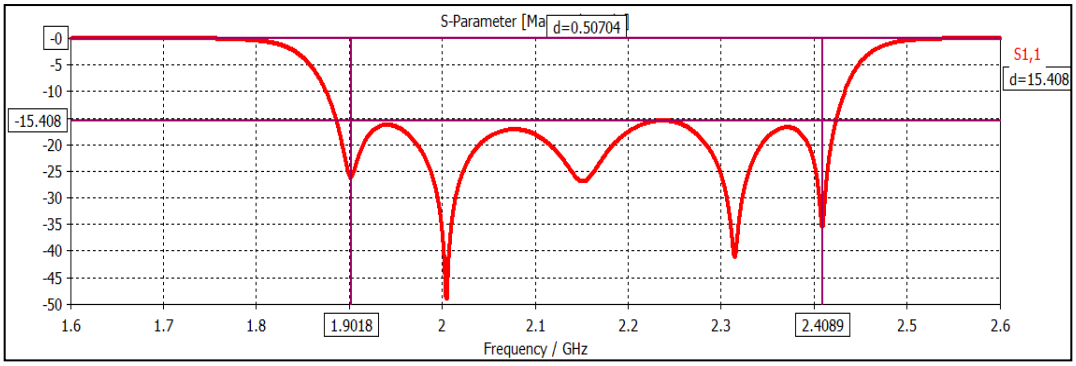

(a)

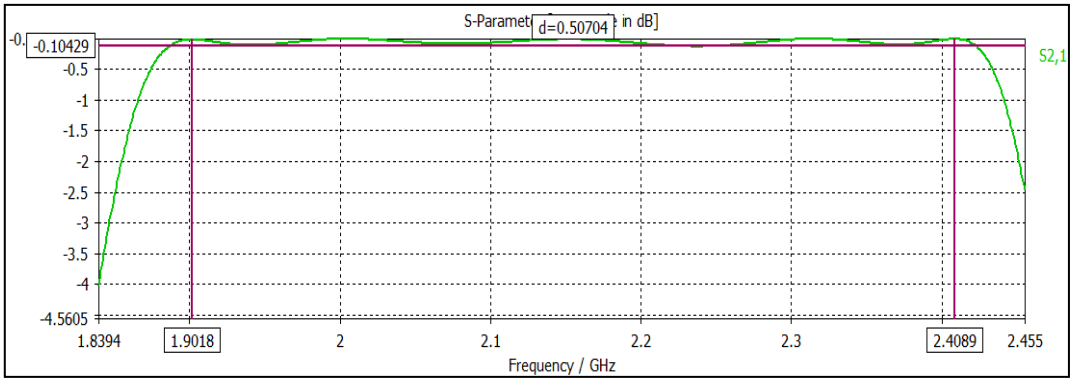

(b)

Figure 4.9: UMTS 5-pole hairpin filter final response (a) S_{11} response (b) S_{21} response.

Table 4.2: UMTS initial and final parameters.

Parameter	Initial value (mm)	Final value (mm)
Spacing between the arms of the resonator (S1)	2	2
Spacing between resonator 1,2 & 4,5 (S2)	0.507597	0.5100223162
Spacing between resonator 2,3 & 3,4 (S3)	0.646088	0.6459310371
Length of the 1st and 5th resonators (P1)	34.2540	33.4244
Length of the 2nd and 4th resonators (P2)	36.8070	35.8779
Length of the 3rd resonator (P3)	36.5476	35.7208

Width of the 1st ,2nd ,3rd, 4th and 5th resonators (W1)	1	1
Width of the feed input/output (W2)	1.85	1.85

4.3 LTE Filter:

A bandpass microstrip 5-pole filter has a fractional bandwidth 7.33% at a center frequency 2.5933 GHz is designed for LTE system. The same RT/ Duroide 6006 substrate used in previous filters is used here. The input/output characteristic impedance of feeding line is 50 Ω and the resonator impedance is 68.3 Ω.

Figure 4.10 shows the design of the filter, and figure 4.11 gives us the initial response.

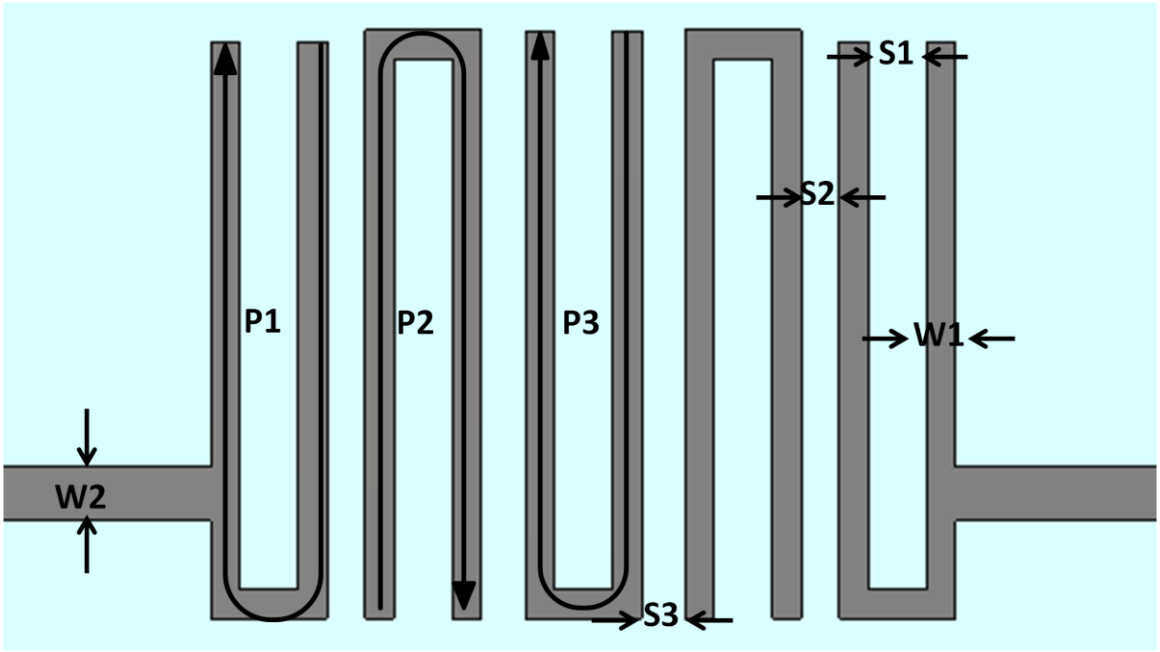

Figure 4.10: LTE 5-pole hairpin filter layout.

As in figure 4.11, the return loss is about -9.6 dB and the passband ripple is about -0.5 dB. This result needs for more modifications on the coupling coefficients, resonator lengths and the external couplings. The final results are depicted in figure 4.12 which give a return loss of about -14.7 dB and a passband ripple of about -0.1 dB, and table 4.4 shows the initial and final parameters.

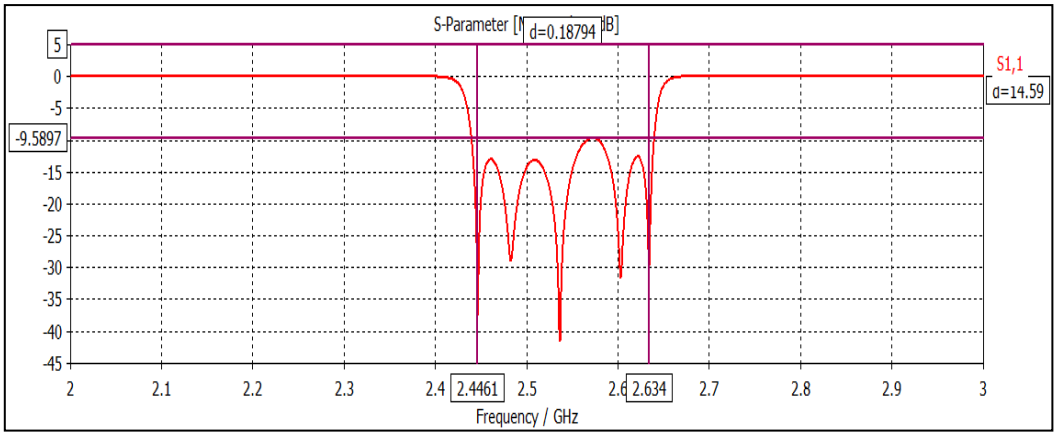

(a)

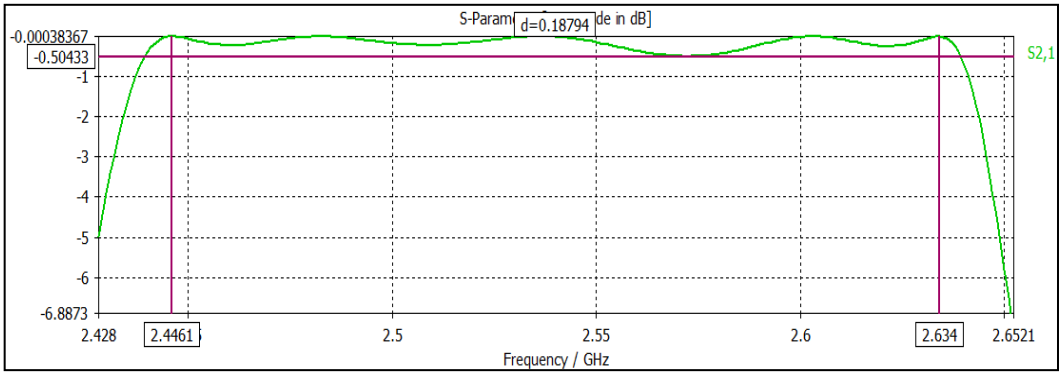

(b)

Figure 4.11: LTE 5-pole hairpin filter initial response (a) S_{11} response (b) S_{21} response.

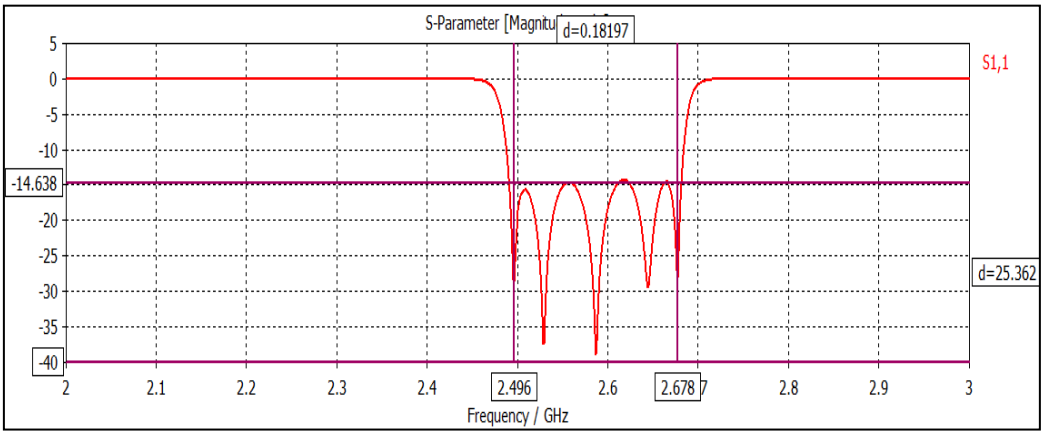

(a)

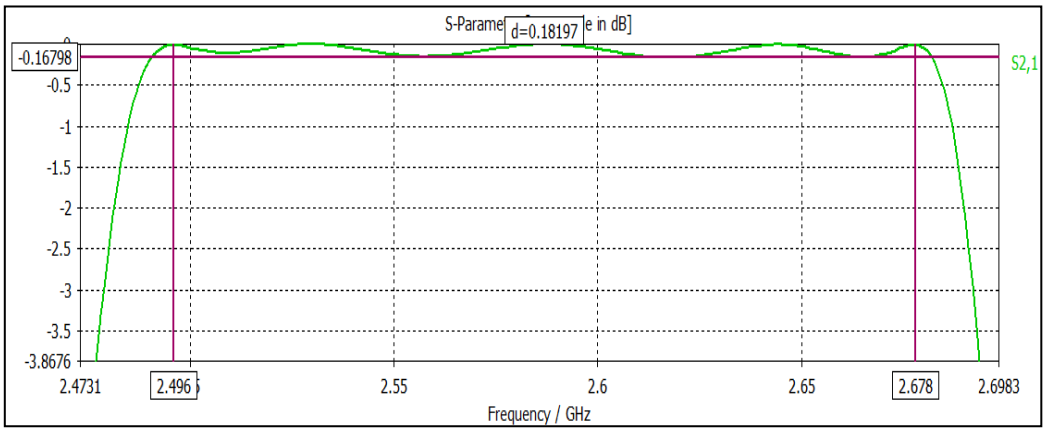

(b)

Figure 4.12: LTE 5-pole hairpin filter final response (a) S_{11} response (b) S_{21} response.

Table 4.3: LTE initial and final parameters.

Parameter	Initial value (mm)	Final value (mm)
Spacing between the arms of the resonator (S1)	2.4505	2.4505
Spacing between resonator 1,2 & 4,5 (S2)	1.639	1.67063
Spacing between resonator 2,3 & 3,4 (S3)	1.94	1.953
Length of the 1st and 5th resonators (P1)	29.7105	29.1505
Length of the 2nd and 4th resonators (P2)	30.0005	29.5038
Length of the 3rd resonator (P3)	29.9905	29.2944
Width of the 1st ,2nd ,3rd, 4th and 5th resonators (W1)	1	1
Width of the feed input/output (W2)	1.85	1.85

Now, after the design of the filters is completed, the design of the whole multiplexer will be shown in the next chapter.

4.4 Summary:

In this chapter, the DCS, UMTS and LTE filters are designed and simulated using CST Microwave studio software. Each filter has been optimized using CST and the simulation

results show good filter performance. These filters will be combined together to form multiplexer as will be presented in the next chapter.

Chapter 5

Multiplexer Design and Simulation

In this chapter we will discuss the multiplexer theory and the practical design of it. Firstly, the design of a diplexer for UMTS and LTE channels will be presented, and then the design of a triplexer for DCS, UMTS and LTE standards will be showed.

5.1 Multiplexer:

Multiplexers are key components of the transceiver for modern wireless or mobile communication systems. Multiplexers are used to multiplex signals of separate frequency bands into composite signals prior to transmission, or to demultiplex compound signals into sub-bands for further processing upon reception [1]. Nowadays, planar circuits are widely used due to their compact size and low integration cost using the printed circuit technology. In multiservice and multiband communication systems, diplexers and triplexers are needed to possess the capabilities of high compactness, light weight, and high isolation [2], but the drawback of its design that it has higher loss and it is difficult to tune after fabrication [3].

Basically, a multiplexer is composed of bandpass filters and associated matching circuits, and thus proper designs of high-performance filters and matching circuits are essential in the development of a multiplexer [2]. Figure 5.1 shows a typical coupling structure of a conventional multiplexer with parallel-coupled bandpass filters.

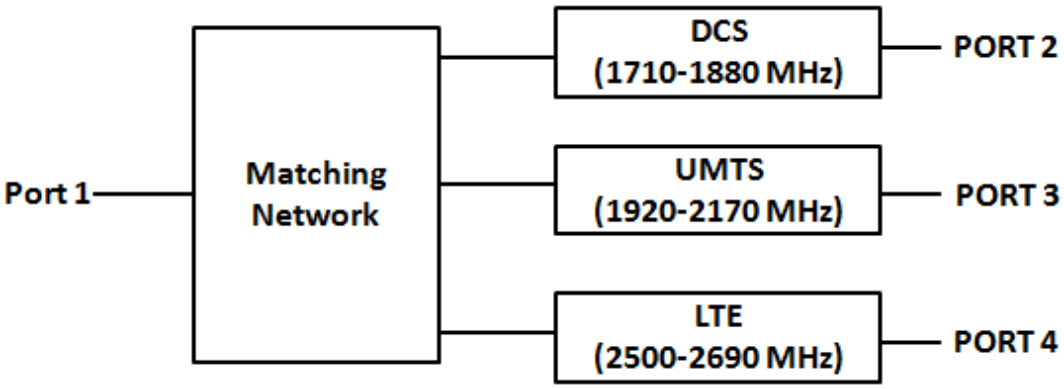

Figure 5.1: conventional multiplexer with parallel-coupled bandpass filters.

Different techniques have been developed to enhance the multiplexer design. The design of multiplexer starts from the lumped-element circuit theory, and moves to the distributed

circuit elements and transmission-line theory, which is more accurate for design and analysis [4]. We remember that inductances and capacitances cause higher loss for the filter circuits so those components are not used for designing a band pass filter. Therefore, microstrip filter structure is designed as a band pass filter [5].

In this thesis, two components are designed; the first is a diplexer for 1920-2170 MHz UMTS and 2500-2690 MHz LTE systems, and the second is a triplexer operating at bands of 1710-1880 MHz DCS, 1920-2170 MHz UMTS and 2500-2690 MHz LTE. The devices are designed by using the Hairpin filters presented in the previous chapter.

The most commonly used distribution configurations are *E*- or *H*-plane *n*-furcated power dividers, circulators and manifold structures [6]. Figure 5.2 shows the configuration of *n*-channel multiplexer with a 1: *n* divider multiplexing network and figure 5.3 depicts a circulator configuration, where each channel consists of a bandpass filter and a channel-dropping circulator [6]. In manifold configurations, channel filters are connected by transmission lines: microstrip, coaxial, waveguide, etc. and T-junctions. The configuration of the manifold multiplexer is shown in figure 5.4 [6]. Based on the advantages of its ability to realize optimum performance for return loss, insertion loss and its compact design, manifold-coupled multiplexers are widely used [4].

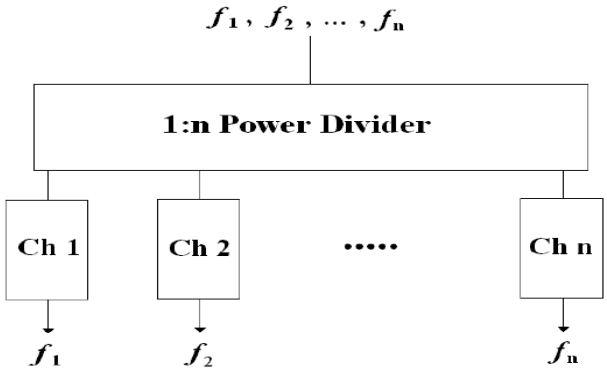

Figure 5.2: Configuration of multiplexer with a 1: n divider multiplexing network.

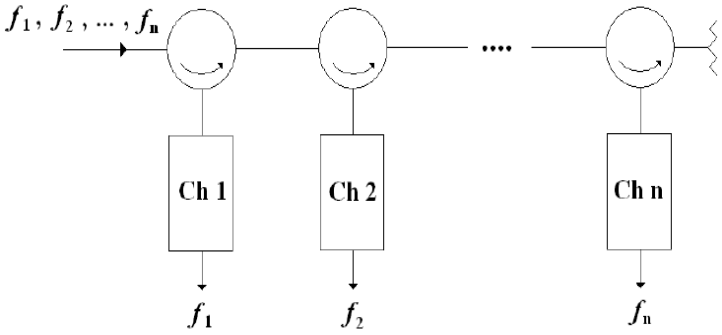

Figure 5.3: Configuration of circulator-coupled multiplexer.

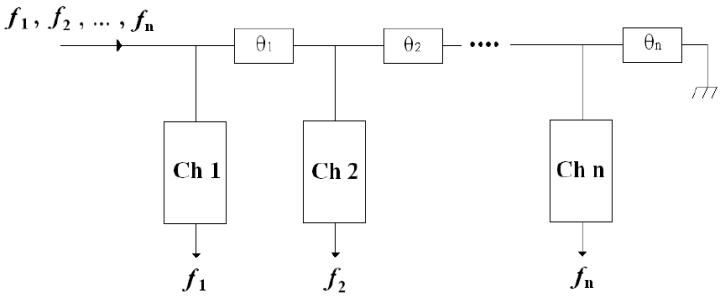

Figure 5.4: Configuration of manifold-coupled multiplexer.

5.1.1 Literature Review:

Many structures of diplexers and triplexers have been proposed in literature. In [7] a novel microstrip diplexer for UMTS and GSM is designed. A microstrip resonator with serial coupling is used to implement this device. As shown in figure 5.5, the modified gap structure allows adjusting the operating frequency of the filters and reduces the size of the device.

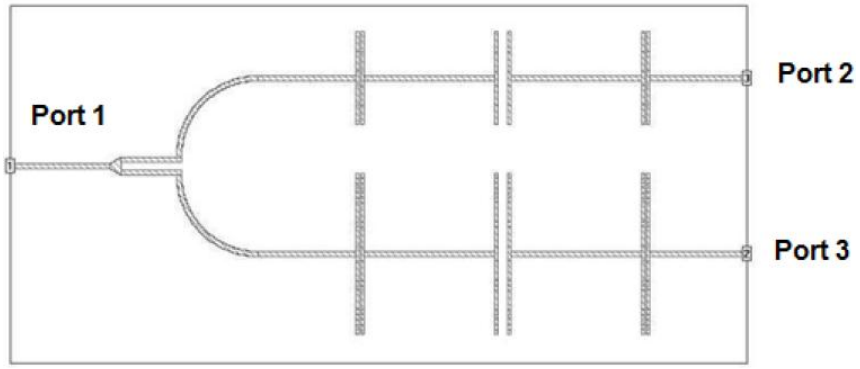

Figure 5.5: Microstrip diplexer for UMTS and GSM [7].

In [8], a square open loop with stepped impedance microstrip resonators are used to implement a compact diplexer, the compact miniaturized two poles square open loop resonators are used to design filters and a diplexer for IMT-2000 bands application as shown in Figure 5.6.

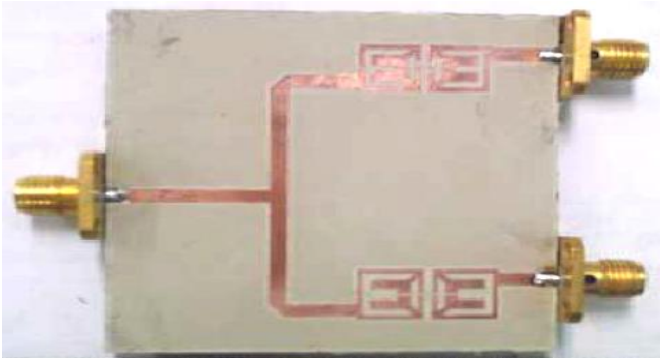

Figure 5.6: A compact diplexer using a square open loop [8].

In [9], a novel microstrip diplexer with a joint T-shaped resonator is proposed. Diplexer is designed to be used in the UMTS-WCDMA system and it has high isolation and wide stopband. By using joint T-shaped resonator the diplexer does not require combining between the circuits and matching networks. The structure is shown in figure 5.7.

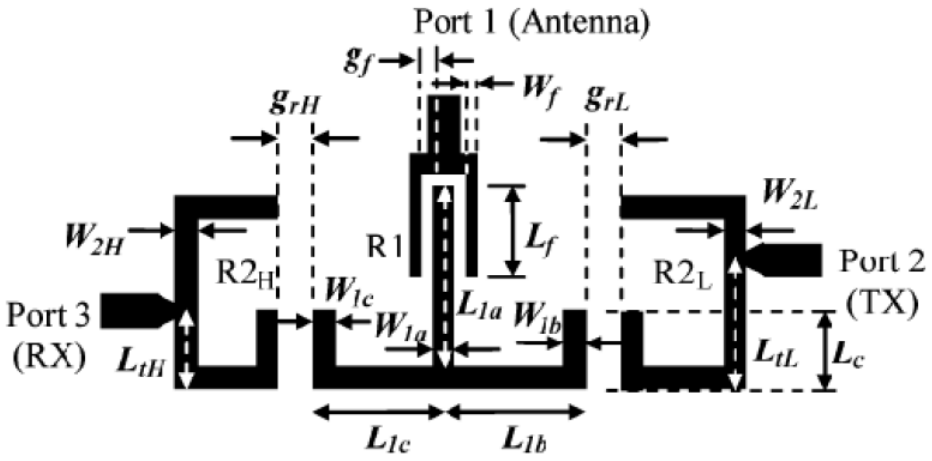

Figure 5.7: the diplexer using the T-shaped resonator, R1, to combine two second-order bandpass filters. Port 1 uses coupled feeding, ports 2 and 3 use tapped feeding [9].

In [10], a microstrip diplexer for UMTS upload and download bands is proposed. The diplexer is based on a two-pole resonator named H-type resonator. This design has a good performance and makes strong use of cross coupling to pass energy between ports. The structure is shown in 5.8.

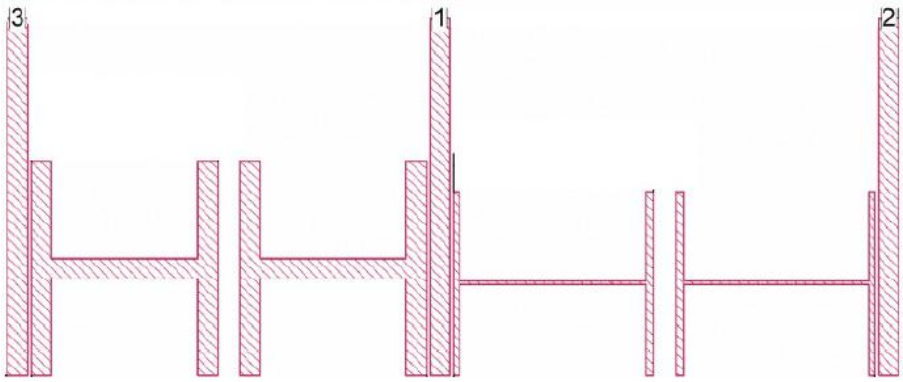

Figure 5.8: A microstrip diplexer for UMTS upload and download bands [10].

In [11], a compact multilayered three-channel multiplexer is proposed. Open-circuited stubs are utilized as wave trapping circuits to provide port isolation. It provides good passband responses and port isolations at all three transmission channels. Figure 5.9 shows the multiplexer structure.

In [12], a compact microstrip triplexer for multiband applications is proposed. In order to

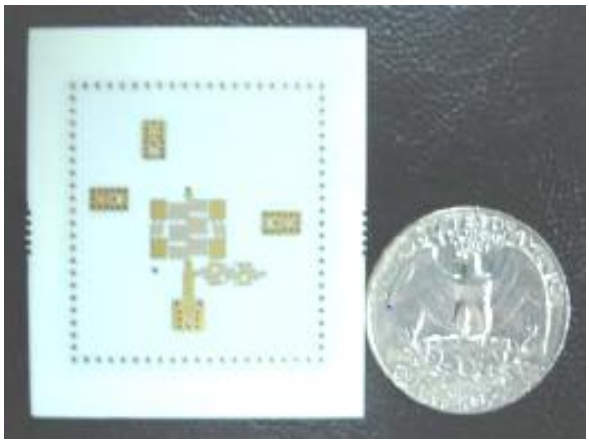

Figure 5.9: Compact Multilayered Three-Channel Multiplexer [11].

achieve compact circuit size and good isolation level, only two stepped impedance resonators (SIRs) and two uniform impedance resonators (UIRs) are used and designed. Figure 5.10 shows the structure.

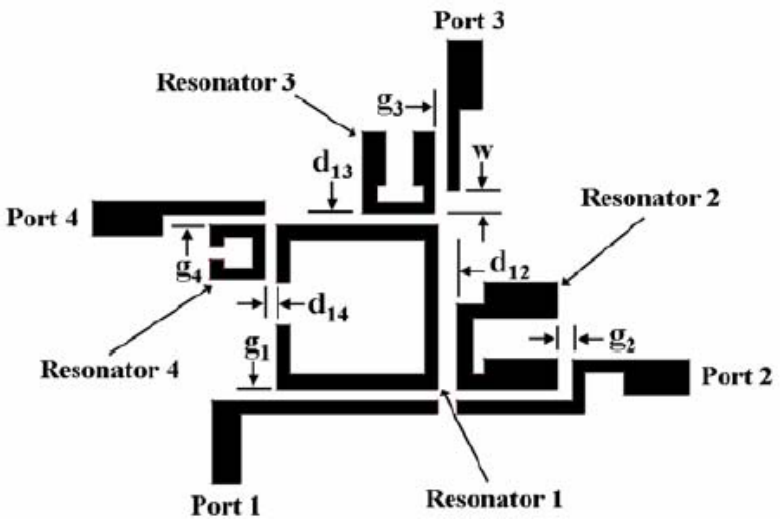

Figure 5.10: Microstrip triplexer for multiband applications [12].

In [13], a frequency triplexer for ultra-wideband systems utilizing combined broadside and edge-coupled filters is proposed. It is verified that this kind of combined broadside- and edge-coupled filters has higher performance than that of conventional edge-coupled filters. The structure is shown in figure 5.11.

In [5], matching circuits for microstrip triplexers are proposed. The triplexer is based on half-wavelength tapped-connected stepped-impedance resonators. The stepped-impedance resonators play important roles for the matching circuits, either to serve as a through pass at the center frequency of a bandpass filter or to provide a short circuit at the center

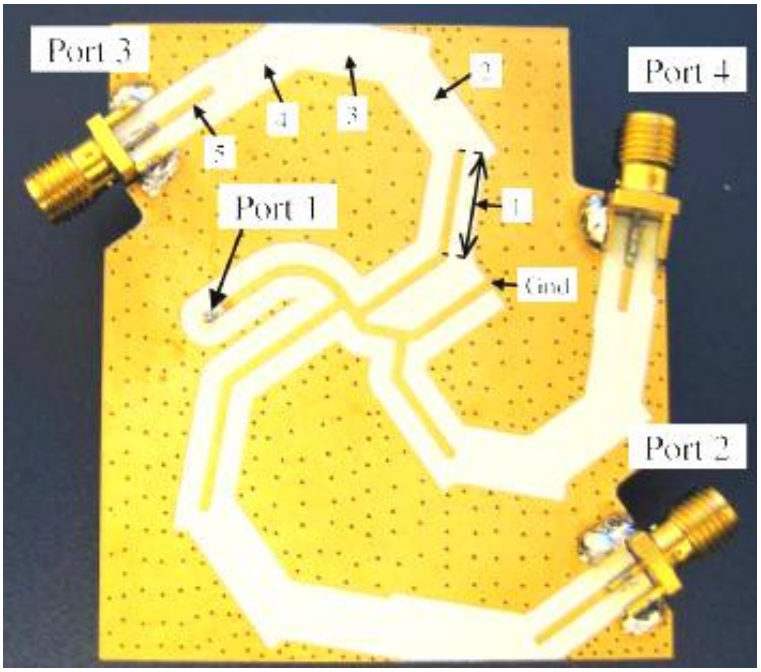

Figure 5.11: A frequency triplexer for UWB systems [13].

frequency of another bandpass filter. The design procedure is simple and the structure is shown in figure 5.12.

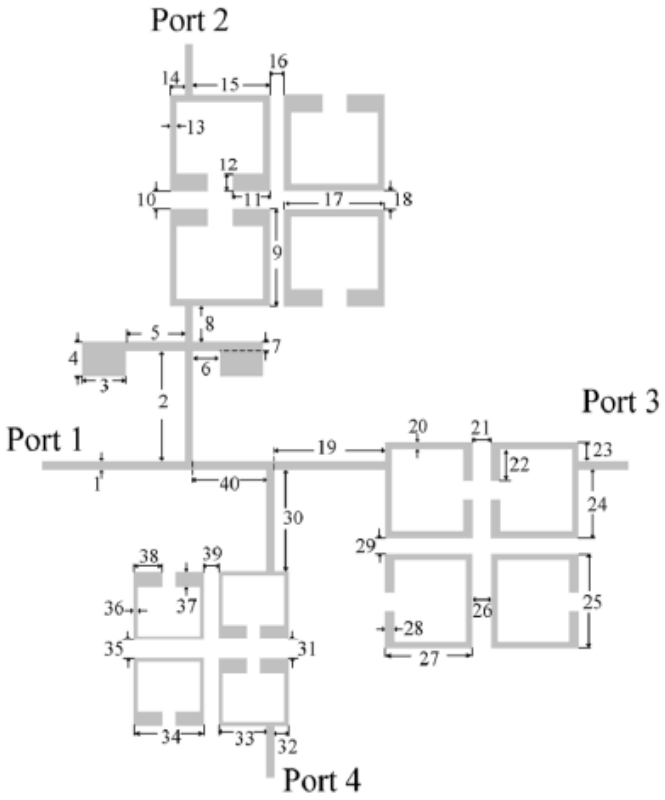

Figure 5.12: Microstrip triplexer [5].

In [14], a ring manifold for connecting microstrip bandpass channel filters to form a multiplexer has been developed. All ports are well matched in their passband, and highly isolated. By modifying the length of the feed lines which connect the filters to the ring, it has been shown that the filters can be connected to the ring to form a multiplexer without significant interaction. Experimental results for the multiplexer are given to verify the technique, and show good agreement with the simulated results. The design is shown in figure 5.13.

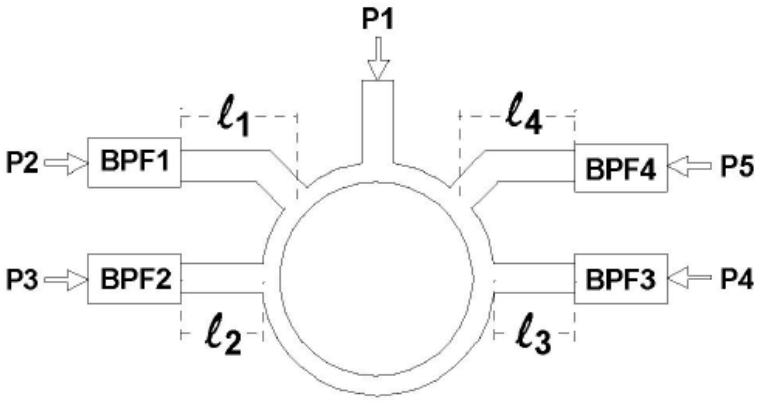

Figure 5.13: Four channel filters connected to a ring manifold [14].

5.1.2: Multiplexer Design:

The design procedure of the proposed multiplexer for mobile communication systems is based on a distributed coupling achieved by central feeding transmission line [15]. Since the uniform resonators would resonate at multiple fundamental frequencies, to obtain high-isolation multiplexers, the resonators are properly located with respect to the input and output feeding lines. Furthermore, because the proposed multiplexer utilizes the distributed coupling technique, the proposed configuration has a high freedom in choosing passband frequencies. Figure 5.14(a) shows the UMTS/ LTE diplexer, while figure 5.14(b) shows DCS/ UMTS/ LTE triplexer. In order to excite the passbands, the couplings between the resonators and the feeding transmission line should be controlled by the parameters X_n $(n = 1,2,3,..)$. Also the vertical distance between the centers of input channels is initially set to $n\lambda/4$ $(n = 1,2, ...)$, and then optimized for better performance.

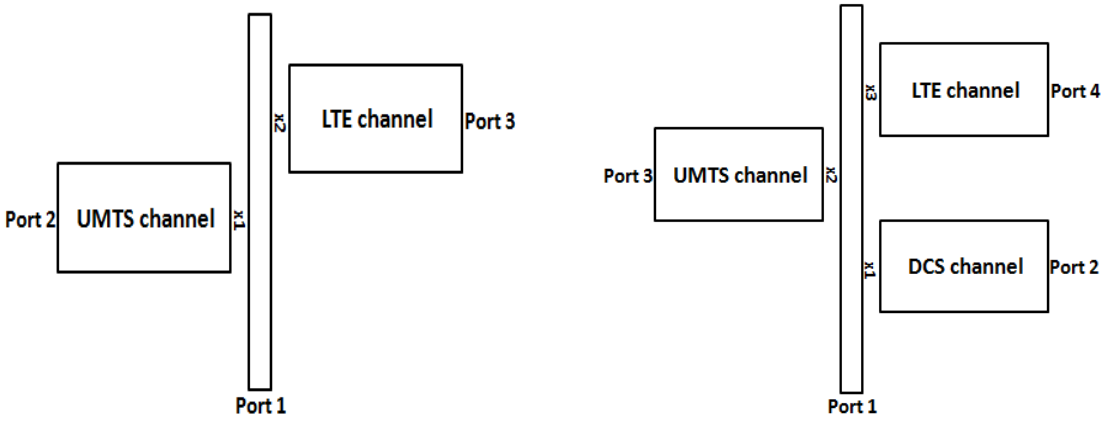

Figure 5.14: Multiplexer design (a) UMTS/LTE Diplexer. (b) DCS/UMTS/LTE Triplexer.

5.1.3 Multiplexer design flowchart:

The complete design procedure of the multiplexer is illustrated by the flowchart in figure 5.15 and is explained step by step as follows:

Step 1: Starts by theoretical design for DCS/UMTS/LTE filters.

Step 2: Design the filters using the CST Microwave studio EM simulator by adjusting the internal and external coupling.

Step 3: Import the filters obtained in step 2 as sub-circuits and couple them to the central feeding line to form the multiplexer.

Step 4: The initial length of the transmission line depends on the wavelength λ designed at lower frequency of the DCS system to the upper frequency of the LTE system (1710-2690 MHz).

Step 5: Set the initial value for location of each filter on transmission line vertically and the value of the gaps for coupling and run to obtain the initial result for the multiplexer.

Step 6: Set the optimization goals and run the optimization with a proper maximum iteration.

Step 7: Verify the optimized result using the EM simulator. If the performance is acceptable, then it is the final design. If it is not acceptable, tune the design using the EM simulator or change the optimization setups slightly within the goals and rerun the optimization.

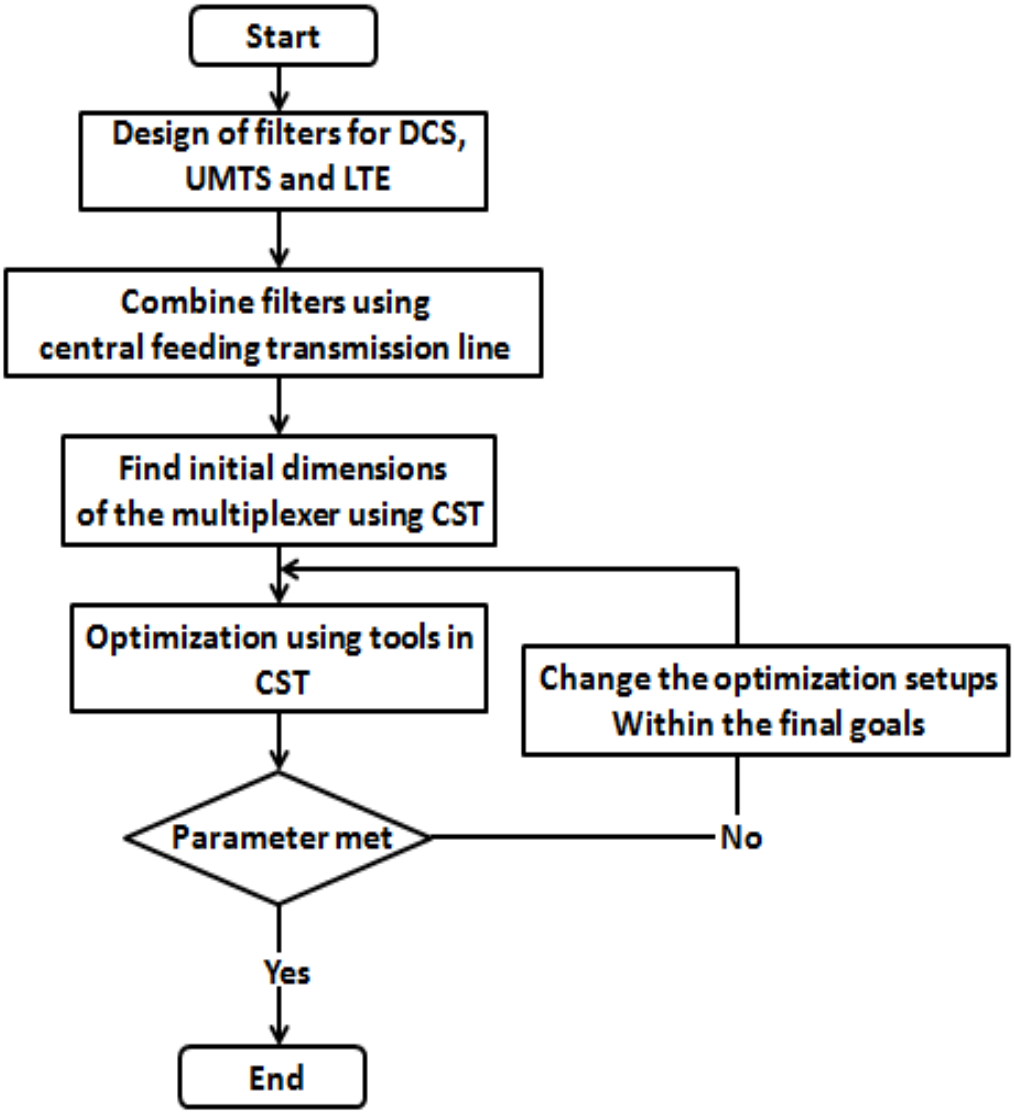

Figure 5.15: Flowchart of multiplexer design.

5.2 DCS/ UMTS/ LTE Triplexer Simulation:

The layout of the final triplexer design and all determined dimensions are illustrated in figure 5.16 and table 5.1 respectively. The triplexer has an overall size of 80.8 × 52.7 mm. To improve the performance of the triplexer, some parameters are controlled. Firstly, control the distance between each channel and the central transmission line shown in figure 5.16 to obtain the best coupling, and then the vertical locations of each distance between filters is controlled.

Figure 5.17 shows the performance of the triplexer. It can be shown from the simulation results that the return loss for the DCS channel is about -7 dB and the insertion loss is about -1.5 dB. Also and the return loss for the UMTS channel is about -8.5 dB and the

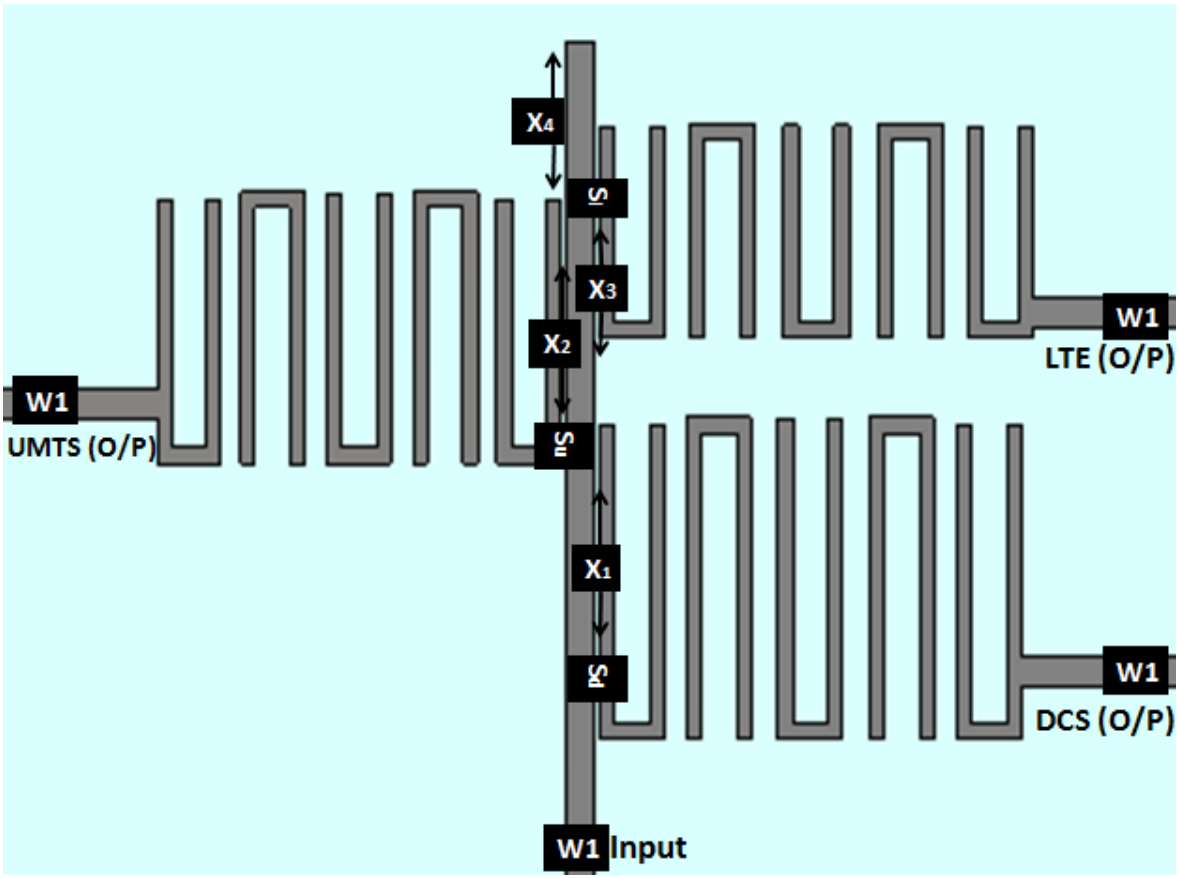

Figure 5.16: Final DCS/ UMTS/ LTE Triplexer layout.

insertion loss is about -1dB, and the return loss for LTE channel is about -7.6 dB and the insertion loss is about -1.2 dB . Moreover, the isolation between DCS, UMTS and LTE is better than 37 dB for DCS and UMTS, while is better than 30 dB for LTE.

Table 5.1: DCS/ UMTS/ LTE triplexer dimensions.

Par. #	Parameter	Value (mm)
1	I/P port (W_1)	1.86
2	DCS O/P port (W_1)	1.86
3	UMTS O/P port (W_1)	1.86
4	LTE O/P port (W_1)	1.86
5	Coupling between DCS filter and T.L (S_d)	0.5229
6	Coupling between UMTS filter and T.L (S_u)	0.3653
7	Coupling between LTE filter and T.L (S_l)	0.4610
8	Location of DCS filter on T.L (X_1)	12.995
9	Location of UMTS filter on T.L (X_2)	29.015
10	Location of LTE filter on T.L (X_3)	34.366
11	Length of the open stub (X_4)	18.366

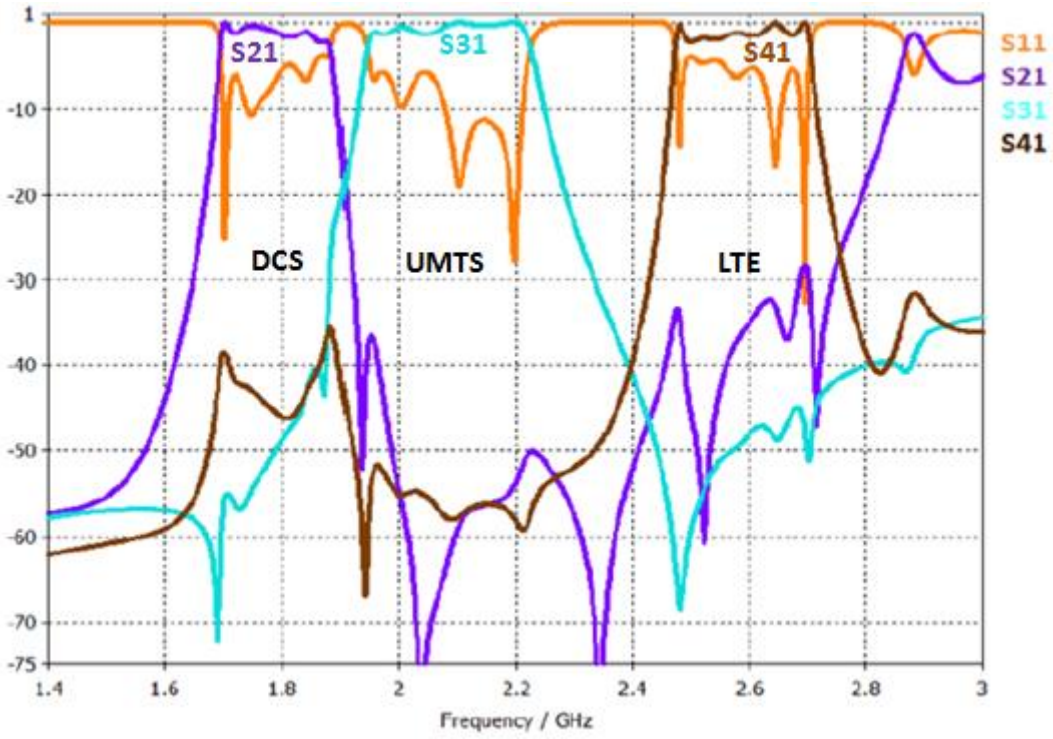

Figure 5.17: The EM simulated performance of the DCS/ UMTS/ LTE Triplexer.

5.3 UMTS/ LTE Diplexer Simulation:

The layout of the final diplexer design and all determined dimensions are illustrated in figure 5.18 and table 5.2 respectively. The diplexer has an overall size of 80.8 × 48.9 mm. To improve the performance of the diplexer, the same procedure for triplexer system is followed.

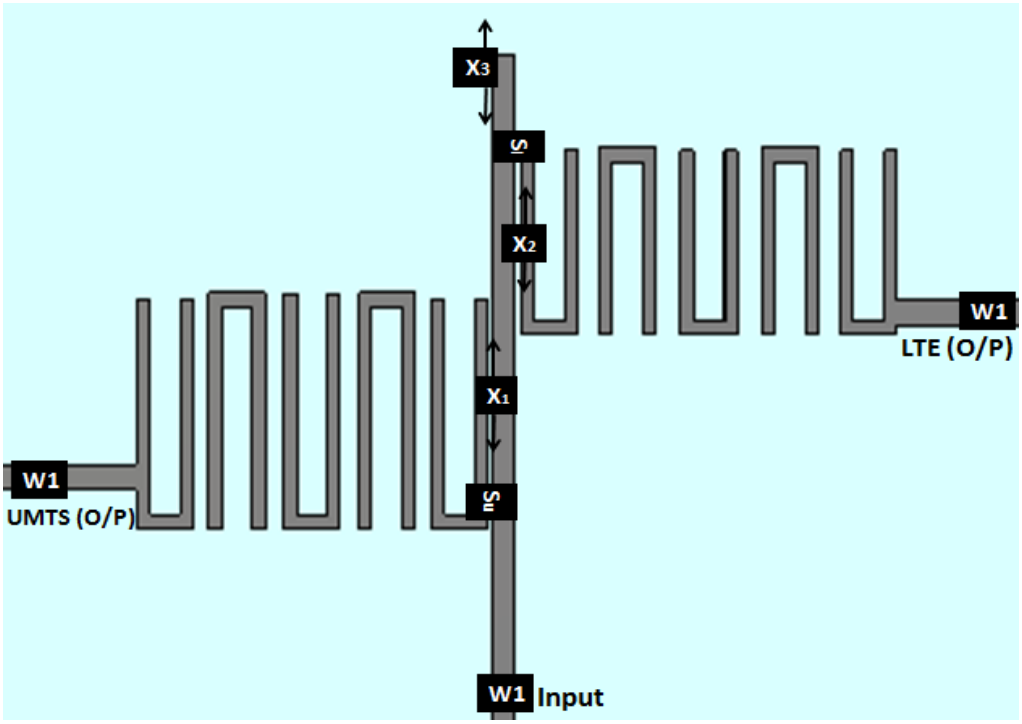

Figure 5.18: Final UMTS/ LTE diplexer design.

Table 5.2: UMTS/ LTE diplexer dimensions.

Par. #	Parameter	Value (mm)
1	I/P port (W_1)	1.86
2	UMTS O/P port (W_1)	1.86
3	LTE O/P port (W_1)	1.86
4	Coupling between UMTS filter and T.L (S_u)	0.3643
5	Coupling between LTE filter and T.L (S_l)	0.4572
6	Location of UMTS filter on T.L (X_1)	18.407
7	Location of LTE filter on T.L (X_2)	30.3
8	Length of the open stub (X_3)	18.693

Figure 5.19 shows the performance of the diplexer. It can be shown from the simulation results that the return loss for the UMTS channel about is -10 dB and the insertion loss is about -0.6 dB, and the return loss for the LTE channel is about -10.2 dB and the insertion loss is about -0.51 dB. The isolation between the two channels is better than 63 dB for DCS and better than 47 dB for UMTS. The result obtained for diplexer is better than that for triplexer since the number of parameters is lower.

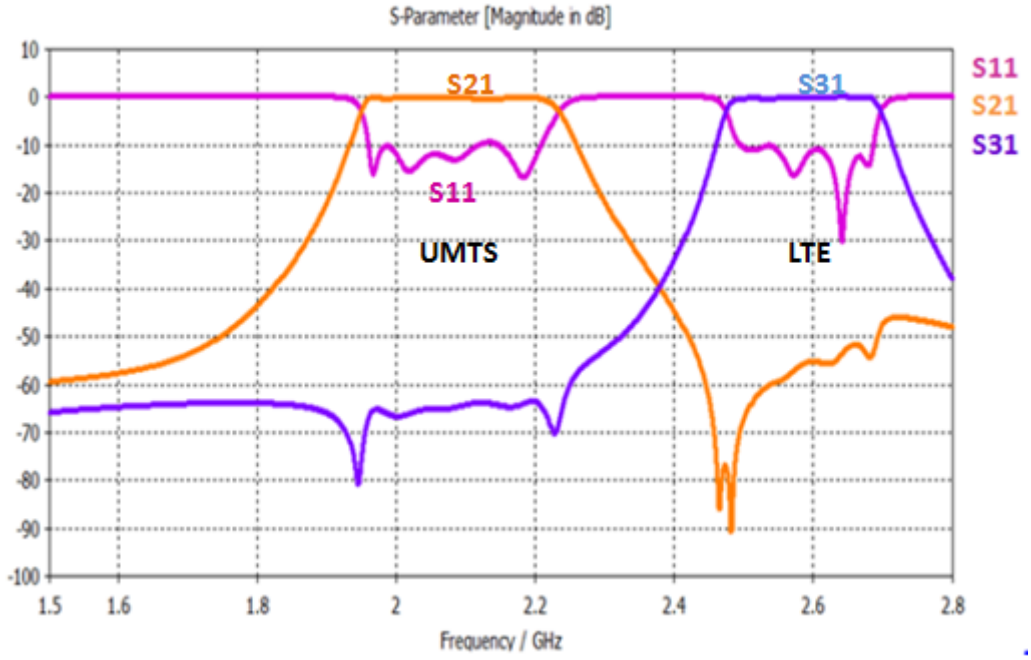

Figure 5.19: The EM simulated performance of the UMTS/ LTE Diplexer.

5.4 Summary:

In this chapter, a compact and high-isolation UMTS/ LTE diplexer and DCS/ UMTS/ LTE triplexer are presented. The design procedure of the components is given. The design is based on coupling individual channel filters to a central feeding transmission line. By locating the filters properly, the insertion loss and isolation can be obtained effectively. The configuration is ready to be applied to multiplexers with more channels.

References:

[1] A. Tunc, C. Ulker, A. Mungan, O. Ceylan, H. Yagci, " Triplexer Design with Hairpin Structure," 19th Telecommunications forum TELFOR 2011," Serbia, Belgrade, pp.22-24, November 2011.

[2] J. Shi, J. Chen and Z. Bao, "Diplexers based on microstrip line resonators with loaded elements," School of Electronics and Information, Progress in Electromagnetics Research, Vol. 115, pp.423-439, 2011.

[3] T. Yang, M. Tamura and T. Itoh, "Compact Hybrid Resonator with Series and Shunt Resonances Used in Miniaturized Filters and Balun Filters," IEEE Transactions on Microwave Theory and Techniques, Vol. 58, No. 2, February 2010.

[4] V. Jadaun, P. Sharma, H. Gupta and D. Mahor, "Design a Microstrip Band Pass Filter for 6 GHz," International Journal of Engineering and Technology, Vol.1, No.3, pp.217-222, 2012.

[5] P. Deng, M. Lai, "Design of Matching Circuits for Microstrip Triplexers Based on Stepped-Impedance Resonators," IEEE Transactions on Microwave Theory and Techniques, vol. 54, no. 12, December 2006.

[6] T. Skaik, "A Synthesis of Coupled Resonator Circuits with Multiple Outputs using Coupling Matrix Optimization", PhD Thesis, March 2011, School of Electronic, Electrical and Computer Engineering, the University of Birmingham.

[7] S. Bezerra, and M. Melo, "Microstrip Diplexer for GSM and UMTS Integration Using Ended Stub Resonators," Proceeding of the IEEE MTT-S International Microwave and Optoelectronics Conference, pp. 954-958, Oct.-Nov. 2007.

[8] J. Konpang, "A Compact Diplexer Using Square Open Loop with Stepped Impedance Resonators," Microwave Conference, 2008. APMC 2008. Asia-Pacific, pp.16-20, Dec. 2008.

[9] M. Chuang, and M. Wu, "Microstrip Diplexer Design Using Common T-Shaped Resonator," Microwave and Wireless Components Letters, IEEE, Vol. 21, Issue: 11, pp. 583 – 585, Nov. 2011.

[10] H. Cabral, S. Bezerra and M. de Melo, "A Diplexer for UMTS Applications," Proceeding of the IEEE MTT-S International Microwave and Optoelectronics Conference (IMOC), pp. 215 – 217, Nov. 2009.

[11] T. Ma, Y. Cheng and J. Tsai, "Compact Multilayered Three-Channel Multiplexer Using Synthesized Microstrip lines and Striplines,"Department of Electrical Engineering, National Taiwan University of Science and Technology, No.43, Keelung Rd. Sec. 4, Taipei 10607, Taiwan, 2011.

[12] H. Wu, K. Shu, R. Yang, M. Weng, J. Chen, and Y. Su, "Design of a Compact Microstrip Triplexer for Multiband Applications," Proceedings of the 37th European Microwave Conference, 2007.

[13] M. Karlsson, P. Håkansson and S. Gong, "A Frequency Triplexer for Ultra-Wideband Systems Utilizing Combined Broadside and Edge-Coupled Filters," IEEE Transactions on advanced packaging, Vol. 31, No. 4, November 2008.

[14] M. Zewani and I. Hunter, "Design of Ring-Manifold Microwave Multiplexers," Institute of Microwave and Photonics, School of Electronic and Electrical Engineering, University of Leeds, Leeds LS2 9JT, UK, 2006.

[15] S. Zeng, J. Wu and W. Tu, "Compact and High-Isolation Quadruplexer Using Distributed Coupling Technique," IEEE Microwave and Wireless Components Letters, Vol. 21, No. 4, April 2011.

Chapter 6

Conclusion and Future Work

6.1 Conclusion:

In this thesis, the generations of the wireless communication systems were studied. The second generation represented by the DCS system operating at the frequency band (1710-1880 MHz), and the third generation represented by UMTS system operating at the frequency band (1920-2170 MHz) and the fourth generation represented by LTE system operating at the frequency band (2500-2690 MHz) were used in the design of the desired components.

The explosive growth and commercial interest in wireless communications, especially in personal and mobile communication systems, significantly increased the demand for low cost, compact size, and high performance triplexers and diplexers. The reduction of the size of the triplexers and diplexers and the need of more stringent specifications, such as high selectivity and low insertion loss, is very important in the design of new products.

The object of the thesis was to develop compact microstrip DCS/ UMTS/ LTE triplexer and UMTS/ LTE diplexer with high performance, which are easy to design and cheap to manufacture.

To obtain these components. Firstly, a simple 5^{th} order microstrip hairpin filter for each band has been designed with good results. For DCS, the return loss is about -15 dB and the insertion loss is about -0.13 dB. For UMTS, the return loss is about -15.5 dB and the insertion loss is about -0.1 dB. For LTE, the return loss is about -14.7 dB and the insertion loss is about -0.1 dB. The second step in the design is to couple the filters designed in the first step to a central transmission line to form the triplexer and diplexer components.

There are different optimization methods used such as Nelder Mead simplex algorithm and Genetic algorithm available in CST microwave studio. Those techniques have been utilized to optimize the diplexer and triplexer components.

For DCS/ UMTS/ LTE triplexer, the return loss for the DCS channel is about -7 dB and the insertion loss is about -1.5 dB, while the return loss for the UMTS channel is about -8.5 dB and the insertion loss is about -1 dB. For the LTE channel the return loss is about -7.6 dB

and the insertion loss is about -1.2 dB. The isolation between DCS and UMTS channels is about -40 dB and between UMTS and LTE channels is about -50 dB.

For UMTS/ LTE diplexer, the return loss for the UMTS channel is about -10 dB and the insertion loss is about -0.6 dB, while the return loss for LTE channel is about -10.2 dB and the insertion loss is about -0.51 dB. The isolation between UMTS and LTE channels is about -63 dB.

6.2 Future Work:

In this work triplexer and diplexer are designed. Further improvement in performance of the triplexer is required using a computer with high specifications. The design of a quadruplexer, composed of four bandpass filters is worthy for further investigation. This design will include four channels for GSM, DCS, UMTS, and LTE systems. There will be a challenge in the design because of the existence of 2^{nd} order harmonic of GSM channel in the other channel bands, and hence harmonic rejection methods are required.

In the future, the designed devices will be fabricated and tested to validate the design results. Unfortunately, fabrication and measurement facilities for microwave components are not currently available at the Islamic university of Gaza, and hence, implementation will be done somewhere else.

There are different structures of microstrip resonators other than hairpin resonator can be used to reduce the dimensions of multiplexers.